Kwinana Air Modelling Study

INTENSIVE EPISODE STUDY 2 WORKSHOP

Papers presented at a workshop
May 16, 1980

DEPARTMENT OF
CONSERVATION & ENVIRONMENT
WESTERN AUSTRALIA

BULLETIN Nº 84

KWINANA AIR MODELLING STUDY

WORKSHOP ON JANUARY 31, 1980 INTENSIVE STUDY

Papers Presented

Held on May 16, 1980 at the Physics

Conference Room, WAIT.

CONTENTS

PREFACE

In order to obtain information on the important sea-breeze phenomena in the Kwinana region, an intensive experiment was carried out on January 31, 1980.

The major component of the study involved the release of two tracer gases from one of the stacks at the SEC power station at Kwinana and the collection of air samples downwind of the release.

Detailed meteorological information was derived from two base stations in the area, one involving the use of an instrumented 27 m tower. In addition data from five anemometers, an acoustic sounder and a number of radiosonde releases were also obtained for the study day.

The release of dense black smoke for short periods alsl enabled aerial and ground photography to be used to accurately determine the direction and rise of the plume.

All of the data collected for the experiment has been compiled in Environmental Note "Kwinana Air Modelling Study - Tracer Experiment 2".

The papers presented in this document were delivered at a KAMS workshop on May 16, 1980 at WAIT. These, and the discussions which followed, were invaluable in terms of understanding the complex problem of pollutant dispersion under sea-breeze conditions in the Kwinana region.

ATTENDANCE

Dr. W. Walker	
Dr. M.J. Lynch	
Dr. P.J. Rye	
Dr. S. Young	Physics Department, WAIT
Ms. P. Kelsey	
Mr. D. Ward	
Mr. P. Glasbergen	
Dr. T. Lyons	School of Environmental and
Dr. W. Scott	Life Science, Murdoch Uni.
Mr. A. Scott	Bureau of Meteorology
Dr. D. Martin	Clean Air Section
Mr. G. Hepworth	Dept. Health & Medical Svs.
Dr. B. Hamilton	
Mr. K. Rayner	Department of Conservation
Mr. J. Rosher	and Environment.
Mr. V. Paparo	

KWINANA AIR MODELLING STUDY

TRACER EXPERIMENT 2 - 31 JANUARY 1980

A. Scott

Meteorology of 31 January

This day was typical of those days during the summer period when a new cooler air mass pushes over the SW of the State following a cool change or, as in this case, when a SE flow is maintained over this region for several days (Fig. 1). The flow in the layer up to 1500 m in the Perth region (Figs 2 and 3) was similar to that at the surface before the sea breeze was established. The 0600 W radiosonde release from Perth Airport showed the base of an inversion layer at a height of about 350 m. At a surface temperature of about 25°C convective mixing would have dissipated this layer.

Maximum temperatures varied significantly across the region (Table 1) and are to some degree directly related to the time of arrival of the sea breeze, however even after the establishment of the sea breeze it is apparent that a significant gradient of temperature existed between the coast and Alcoa's F Lake as Rottnest reported a maximum of 24°C while in the early afternoon temperatures between 27 and 28.7 were observed at F Lake.

Location	Minimum	Maximum
Rottnest	17	24
Hope Valley		~ 26
Alcoa F Lake		~ 28.7
Perth	17.4	28.3 (12.20 pm)
Perth Airport	14	31
Mandurah	15	28

Table 1 Maximum and minimum temperatures in the region.

Ground temperatures at 1 cm depth and the corresponding screen temperatures at F Lake are set out in Table 2.

Screen Temperature	1 cm Ground Temperature	Time
28.7	51	1240
27.1	51	1255
27.9	51	1345
27.5	50.5	1425
27.5	49.2	1455
25.7	47.7	1530
26.3	46.1	1555

The sea breeze developed during the mid morning with a SW wind change being recorded on the northern end of Garden Island at 1000 W. The absence of wind data between Garden Island and the eastern shore of Cockburn Sound precludes any positive statement about the area in which the sea breeze circulation initially developed, however it seems that it was probably west of Garden Island. The streamline charts (Figs 4-7) have been analysed on this basis. At 1400 and 1500 W the analyses are similar to that at 1300. The rate of eastward movement of the sea breeze between 1000 and 1300 was about 1.8 m/sec given the assumption about its initial position of development.

Meteorological Conditions During the Tracer Release and Sampling Period

During this period a fairly steady sea breeze from 220° at between 7-10 m/sec occurred over the Kwinana-Wattleup area at ground level (Fig. 8). The low level radiosonde flights from Alcoa's F Lake revealed a directional shear with height so that at 300 m the wind direction was about 210° and through the layer between 300 and 500 m this changed to about 150° (Fig. 9).

The thermal structure detected by the radiosonde flights (Fig. 10) shows a strengthening and rising inversion layer which during the tracer period lay between 300 and 350 m above ground level at Alcoa's F Lake (345-395 m above Australian Height Datum). The inversion layer coincided with the shear between the sea breeze inflow layer and the overriding SSE/SE winds. Super adiabatic lapse rates existed in the layer below about 130 m with lapse rates near the dry adiabatic between this level and the inversion base.

Interpretation of the acoustic sounder record from the Hope Valley site (Fig. 11) shows a mixing depth of about 400 m during the tracer period.

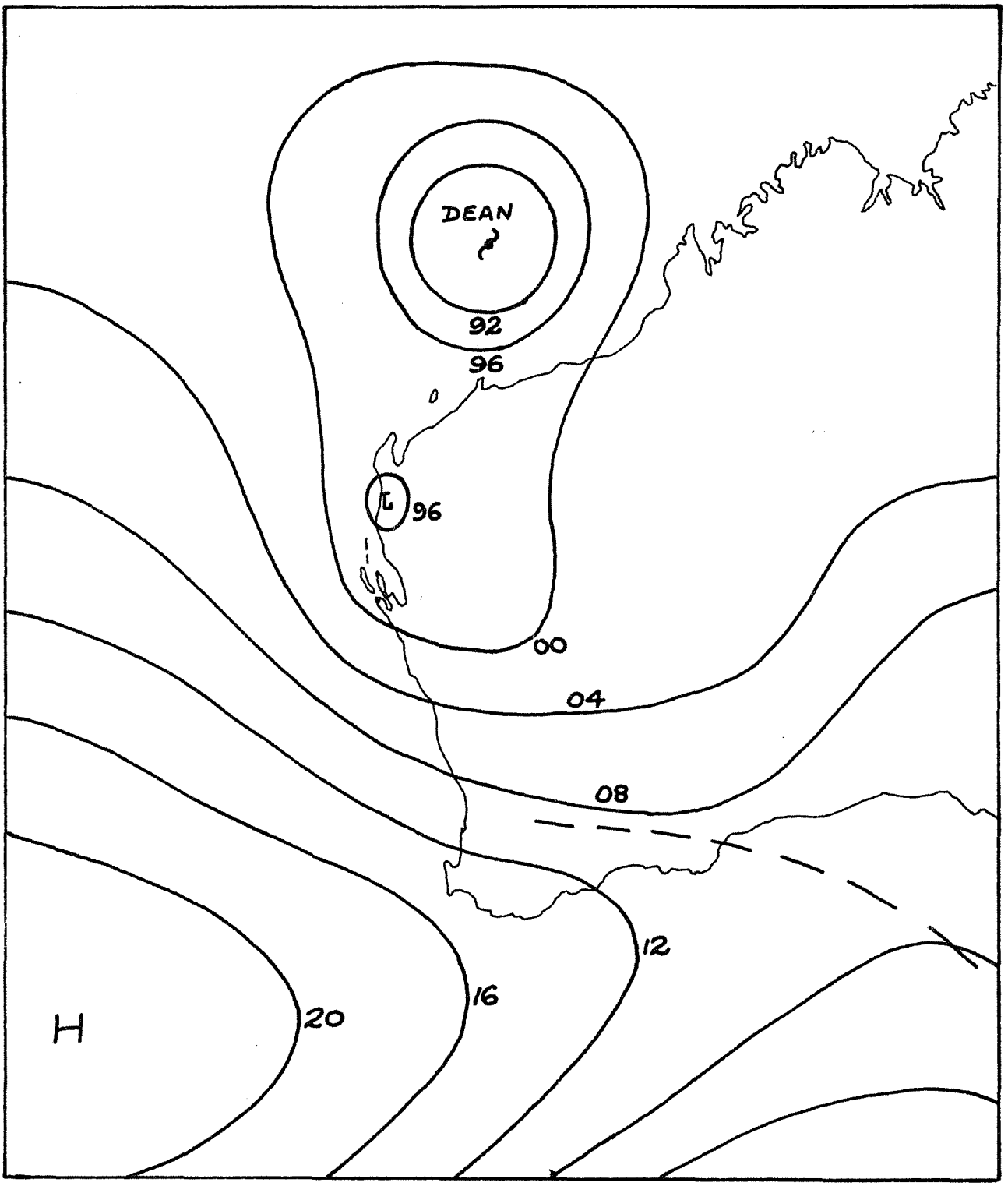

FIGURE 1 Mean sea level analysis 1500 WST 31 January 1980

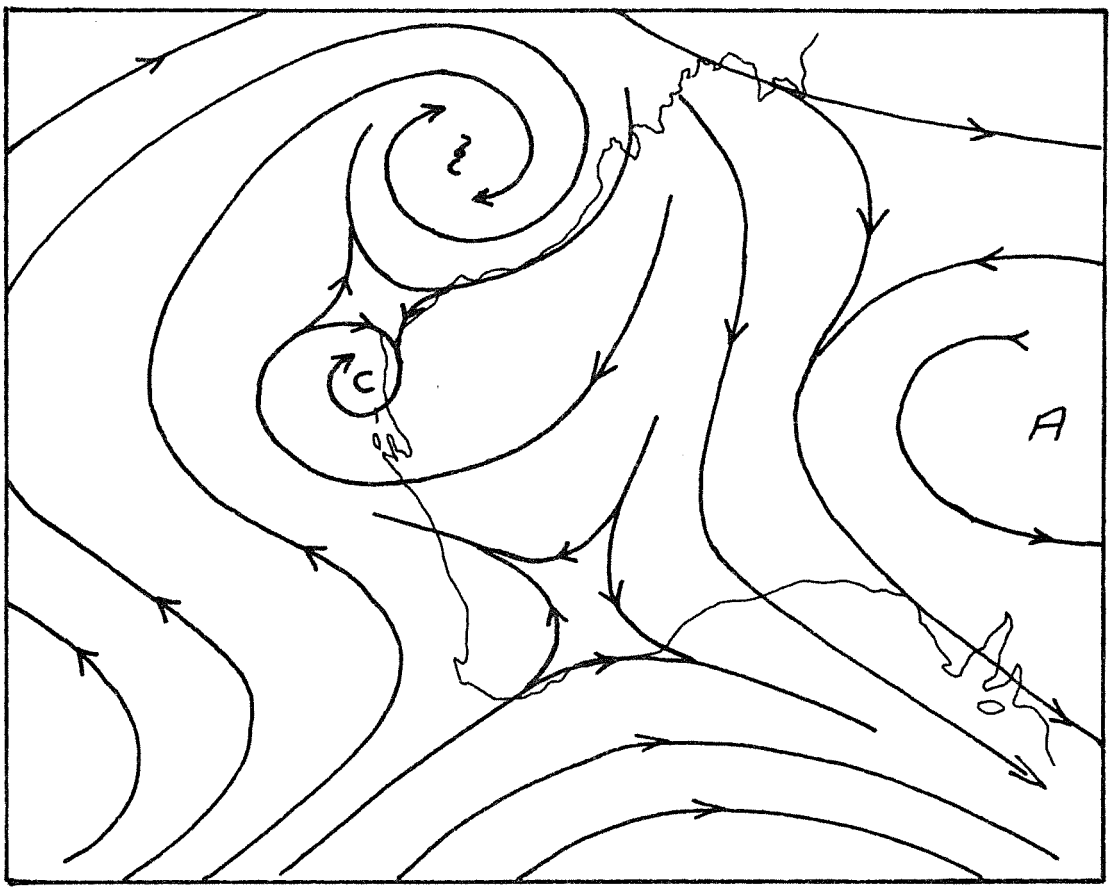

FIGURE 2 900 m streamline analysis
1200 WST 31 January 1980

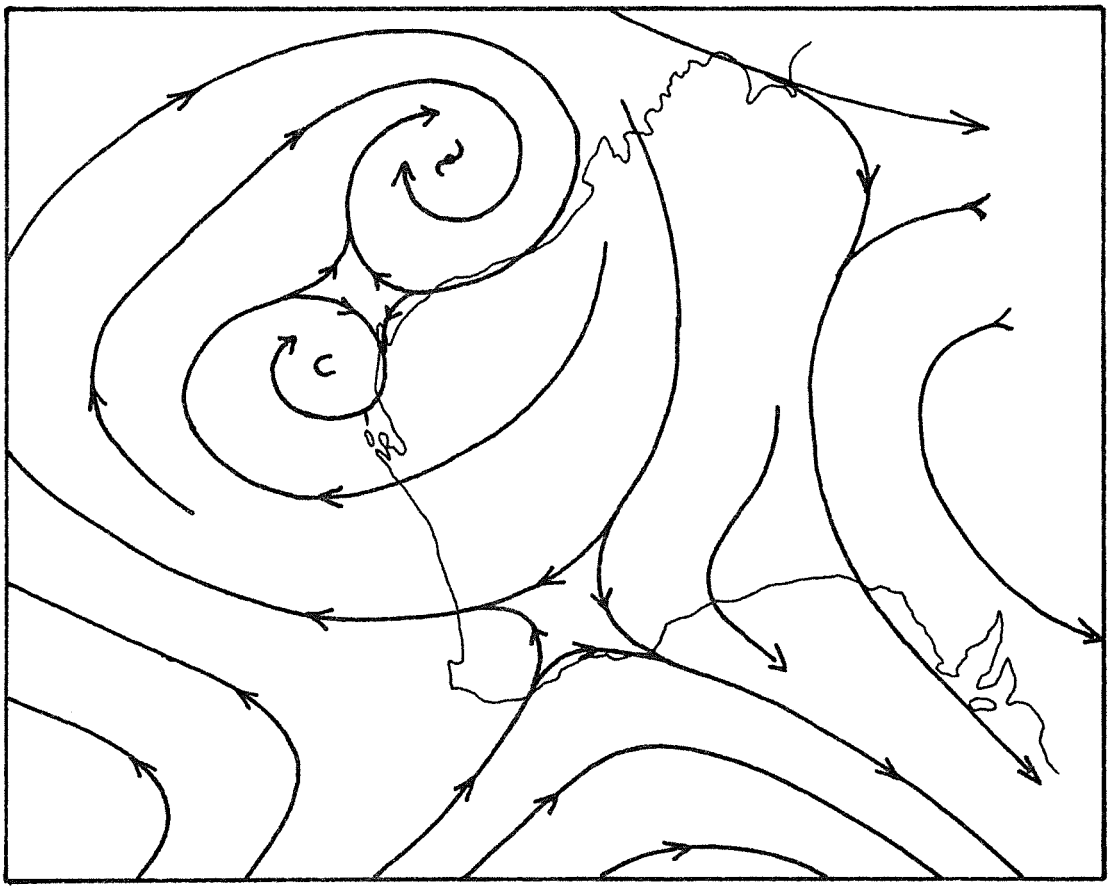

FIGURE 3 1500 m streamline analysis
1200 WST 31 January 1980

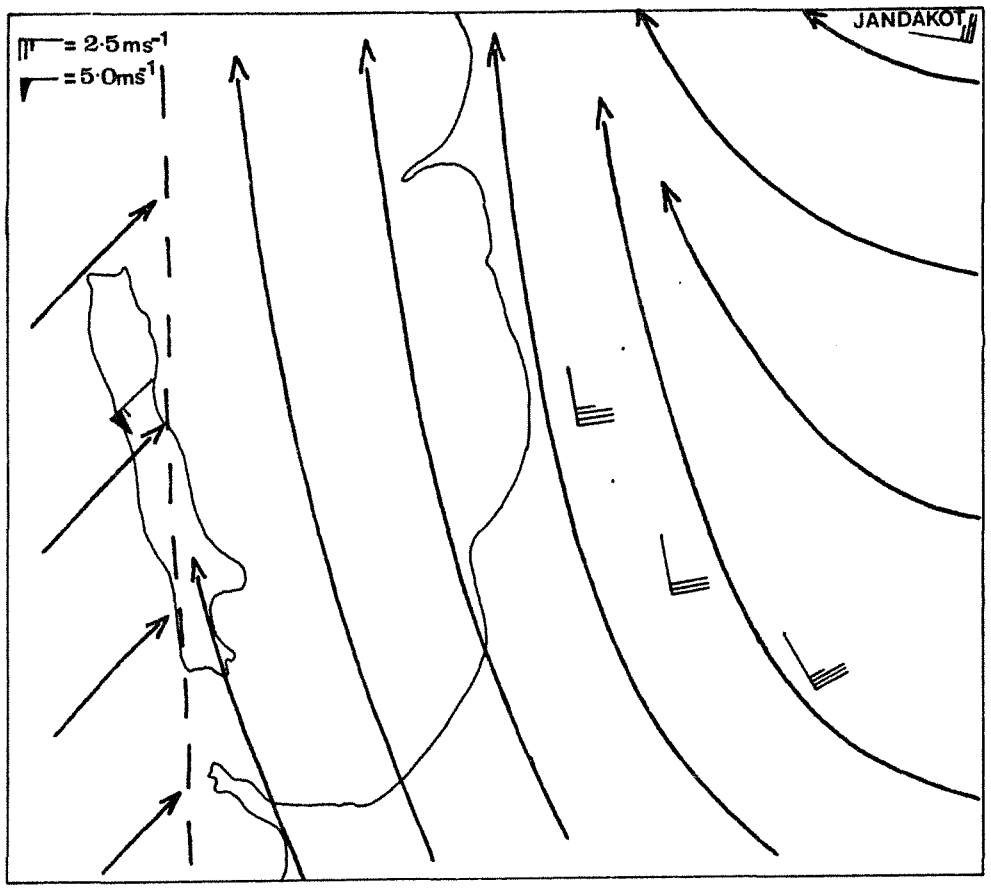

FIGURE 4 Streamline analysis for the Cockburn Sound-Kwinana area 1000 WST 31 January 1980

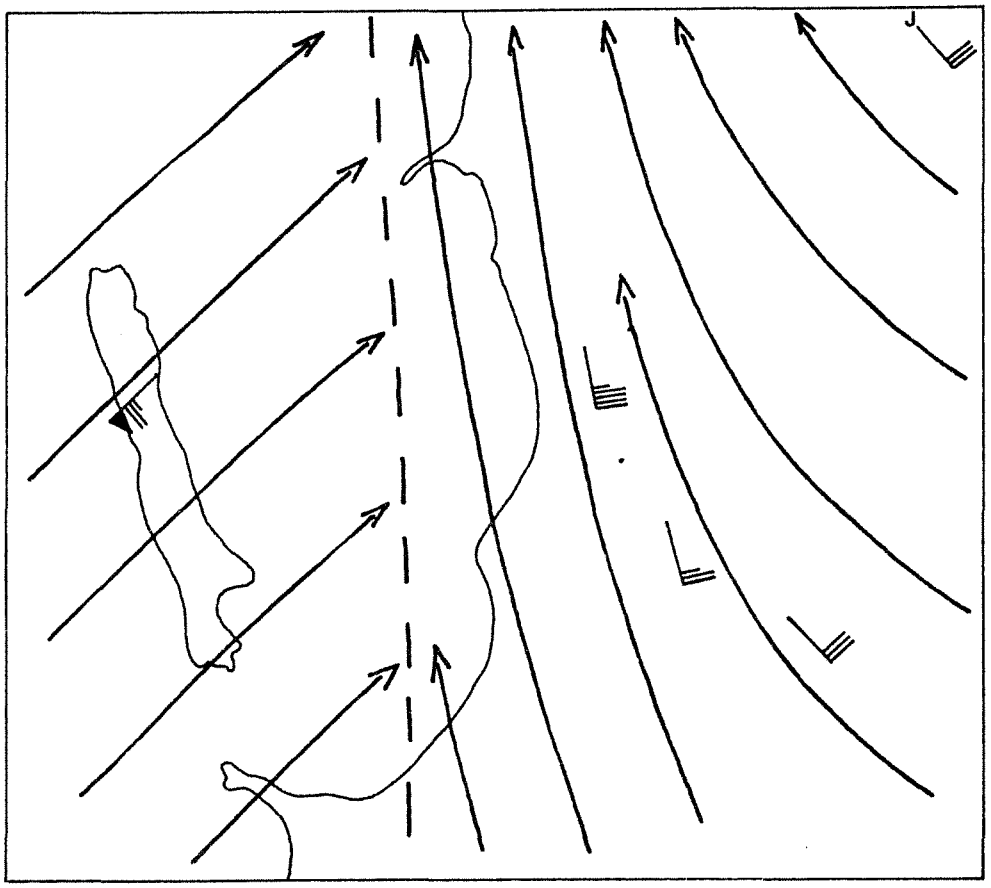

FIGURE 5 Streamline analysis 1100 WST 31 January 1980

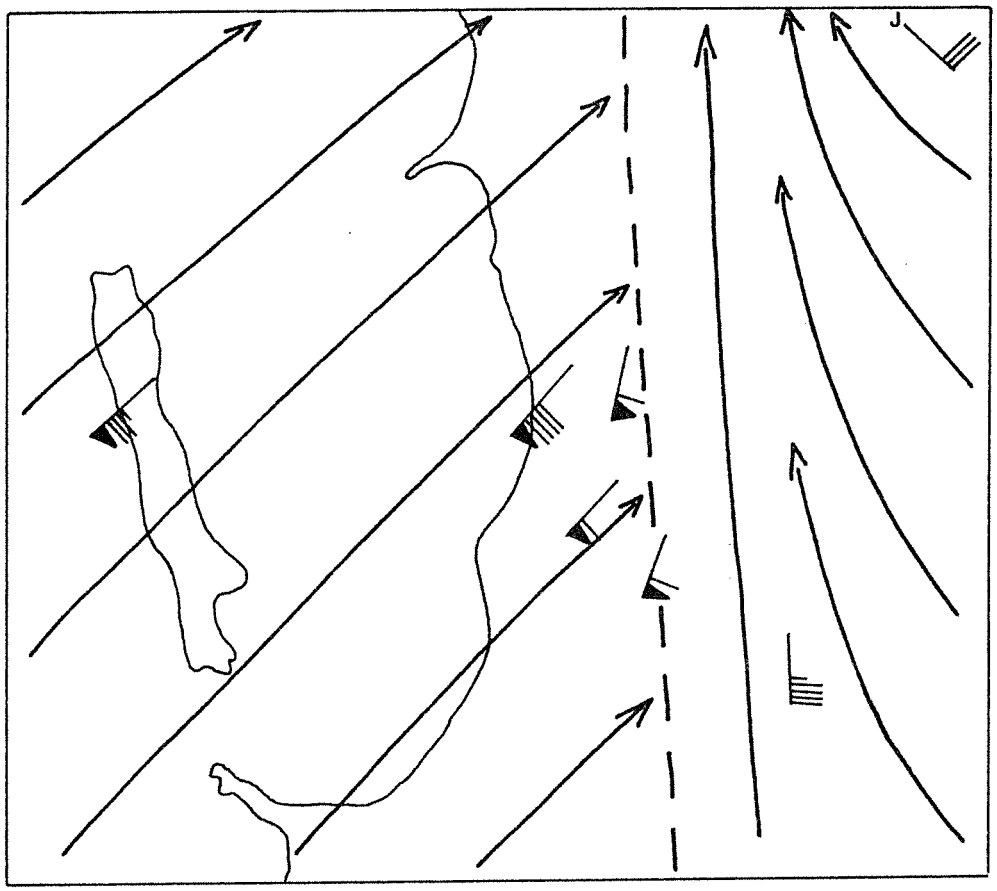

FIGURE 6 Streamline analysis for the Cockburn Sound-Kwinana area 1200 WST 31 January 1980

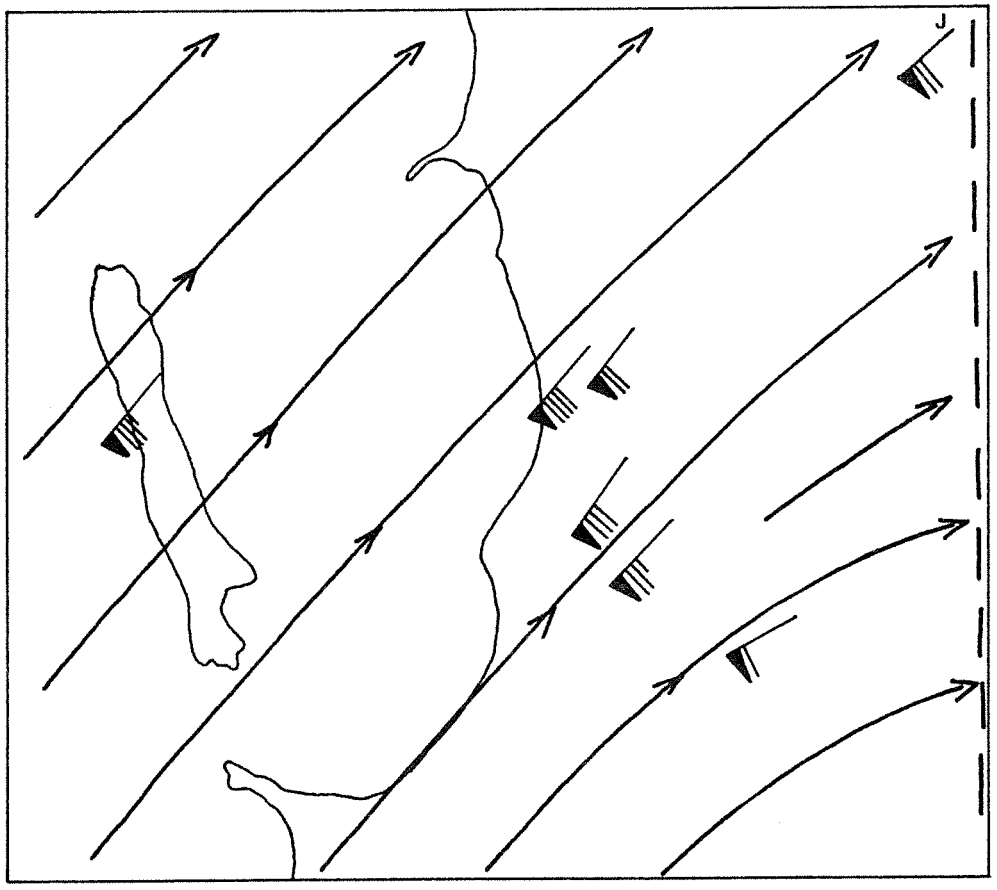

FIGURE 7 Streamline analysis 1300 WST 31 January 1980

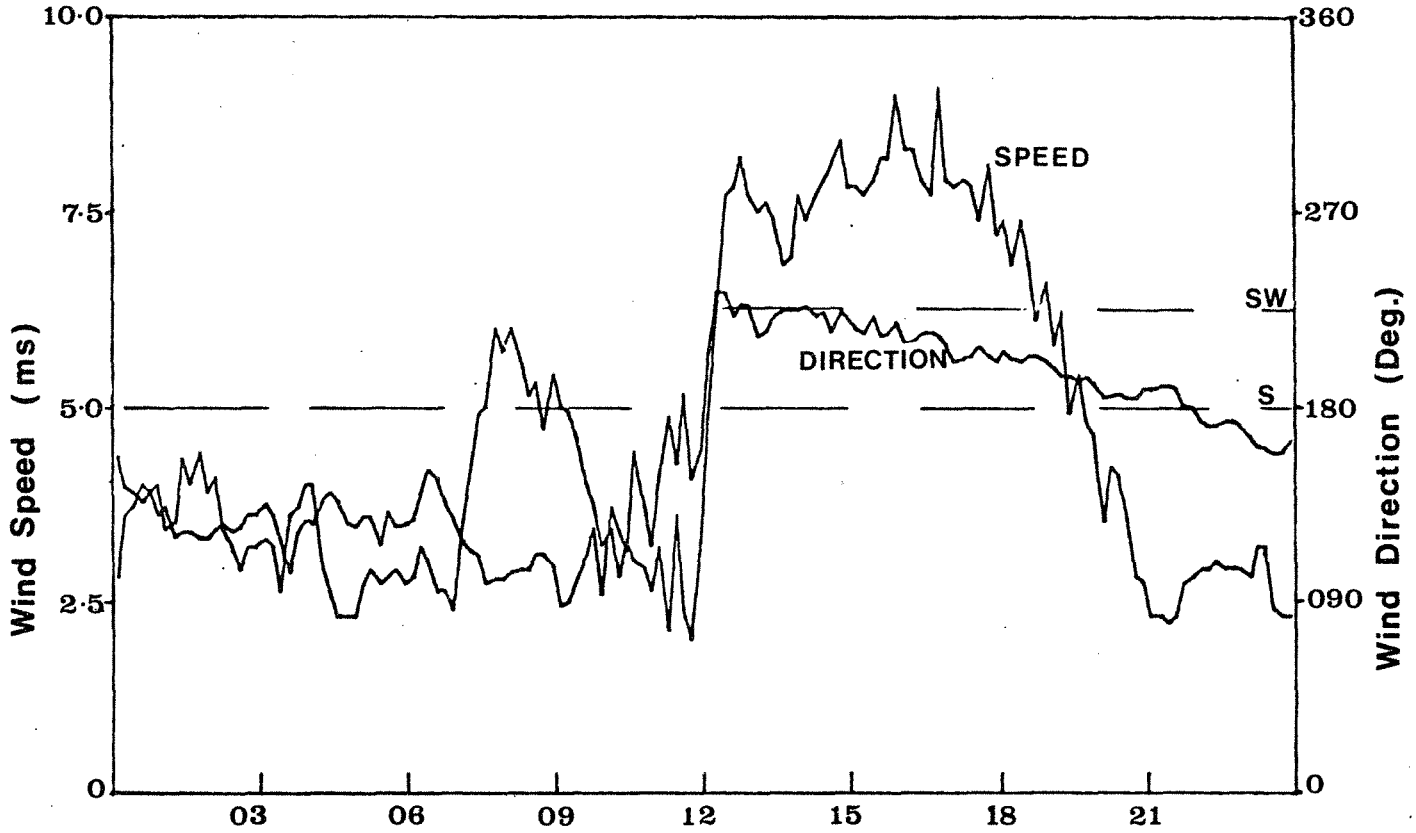

FIGURE 8 Wind direction and speed at the Wattleup Base Station during 31 January 1980

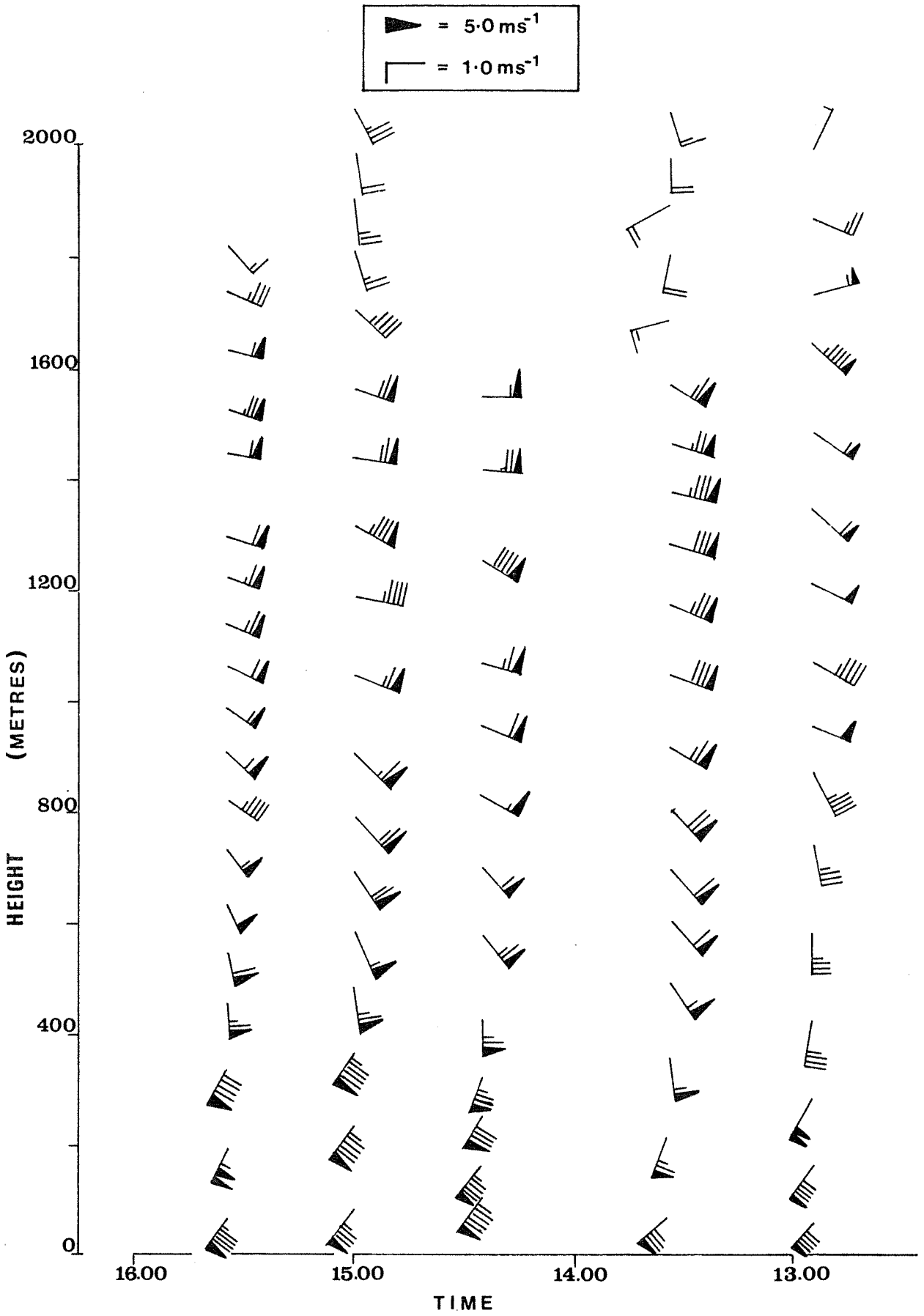

FIGURE 9 Low level winds measured at Alcoa's F Lake
31 January 1980

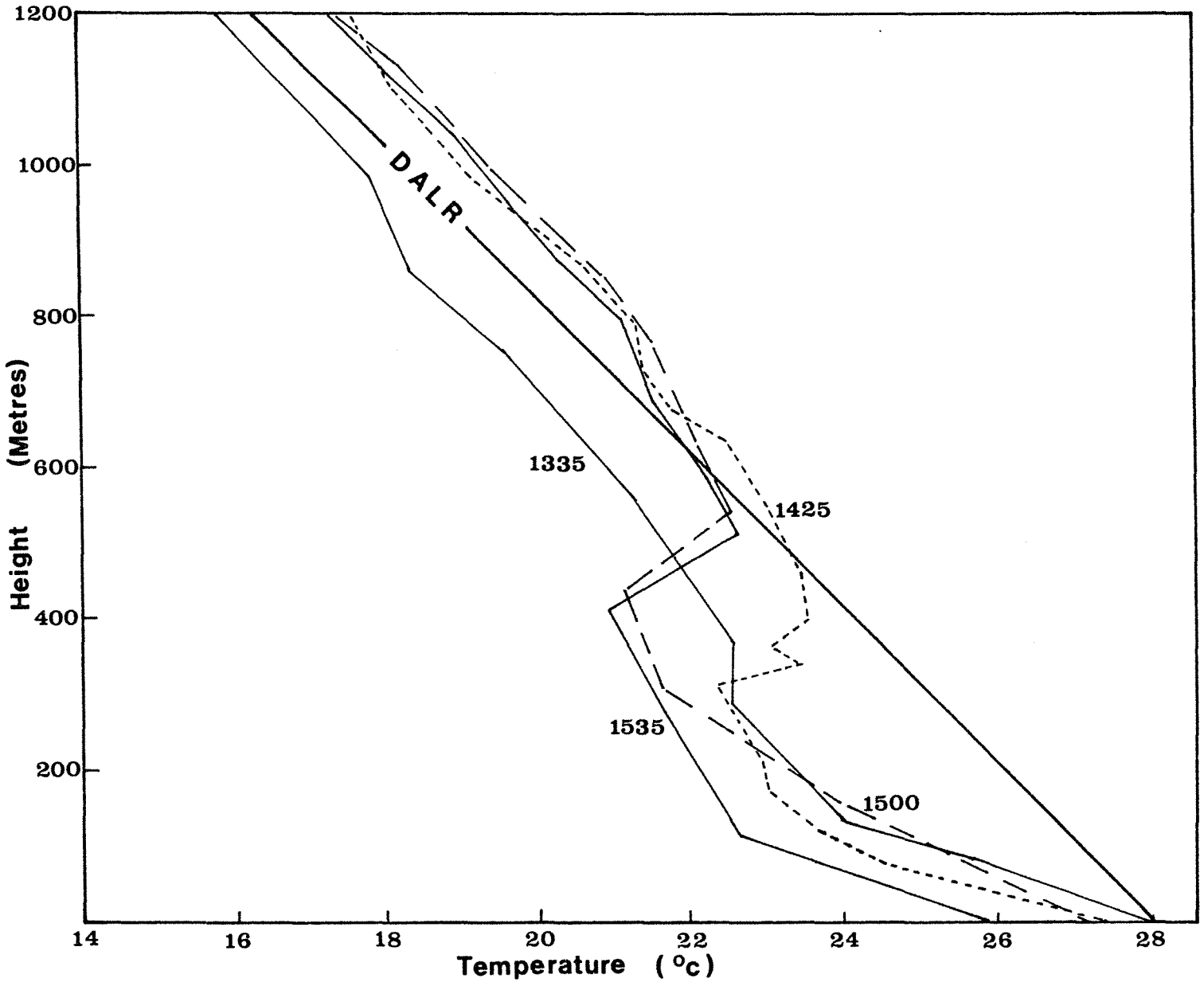

FIGURE 10 Low level temperature data measured at Alcoa's F Lake
31 January 1980

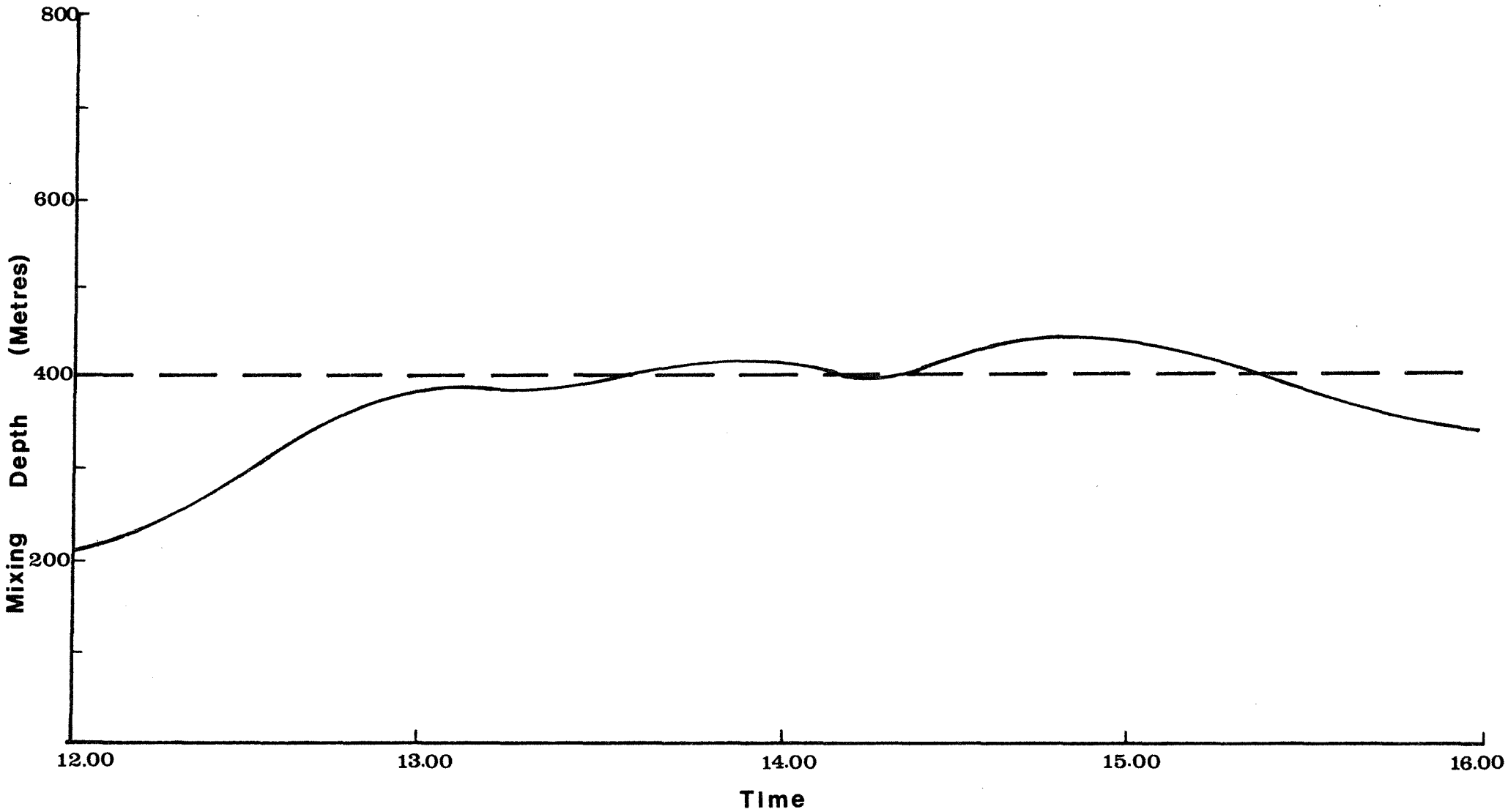

FIGURE 11 Acoustic Sounder record at Hope Valley Station during the afternoon of 31 January 1980

KWINANA AIR MODELLING STUDY

SOME OBSERVATIONS ON THE TRACER EXPERIMENTS

B. H. HAMILTON

1. INTRODUCTION

Three major tracer studies have taken place using the SEC's Kwinana Power Station as the release point. They are :

Coogee Air Pollution Study (CAPS)
5 December 1973
Kwinana Air Modelling Study (KAMS 1)
2 March 1978
Kwinana Air Modelling Study (KAMS 2)
31 January 1980

For the CAPS release only Freon 11 was used while both Freon 11 and sulphur hexafluoride were used in the KAMS releases.

From independent analysis and comparison of the three releases it is possible to make several relevant observations.

2. GENERAL OBSERVATIONS

The use of Freon 11 tracer is fraught with some difficulty as background levels can vary considerably. For example, background measurements of Freon 11 made in January 1977 at a number of sites around the Metropolitan Area varied from around 1 $\mu g/m^3$ to 145 $\mu g/m^3$.

Freon 11 is widely used as a refrigerant and in pressure packs so that urban, commercial and industrial sources can be expected. Experience at Kwinana, at least in the days of CAPS, led us to believe that background Freon 11 levels were quite low ($< 1 \mu g/m^3$) under sea breeze conditions. More recent experience tends to suggest otherwise.

The use of sulphur hexafluoride (SF_6) as a tracer is preferred, as background levels are virtually nonexistent. SF_6 when used in conjunction with Freon 11 can help to distinguish spurious sources of the latter tracer. The known ratio of Freon 11 to SF_6 in the release is used to distinguish Freon 11 originating from the study and that from other sources, as shown below.

With the above knowledge careful examination of the tracer release data can then lead to a series of very useful observations that may be relevant to the modelling part of the exercise.

3. CAPS

Contours developed from the CAPS tracer release are shown in Figure 1. The release rate of Freon 11 was 54.2 g/sec, the wind speed 6 m/sec and the wind direction 220°. Thus CAPS was under very similar conditions to KAMS 1.

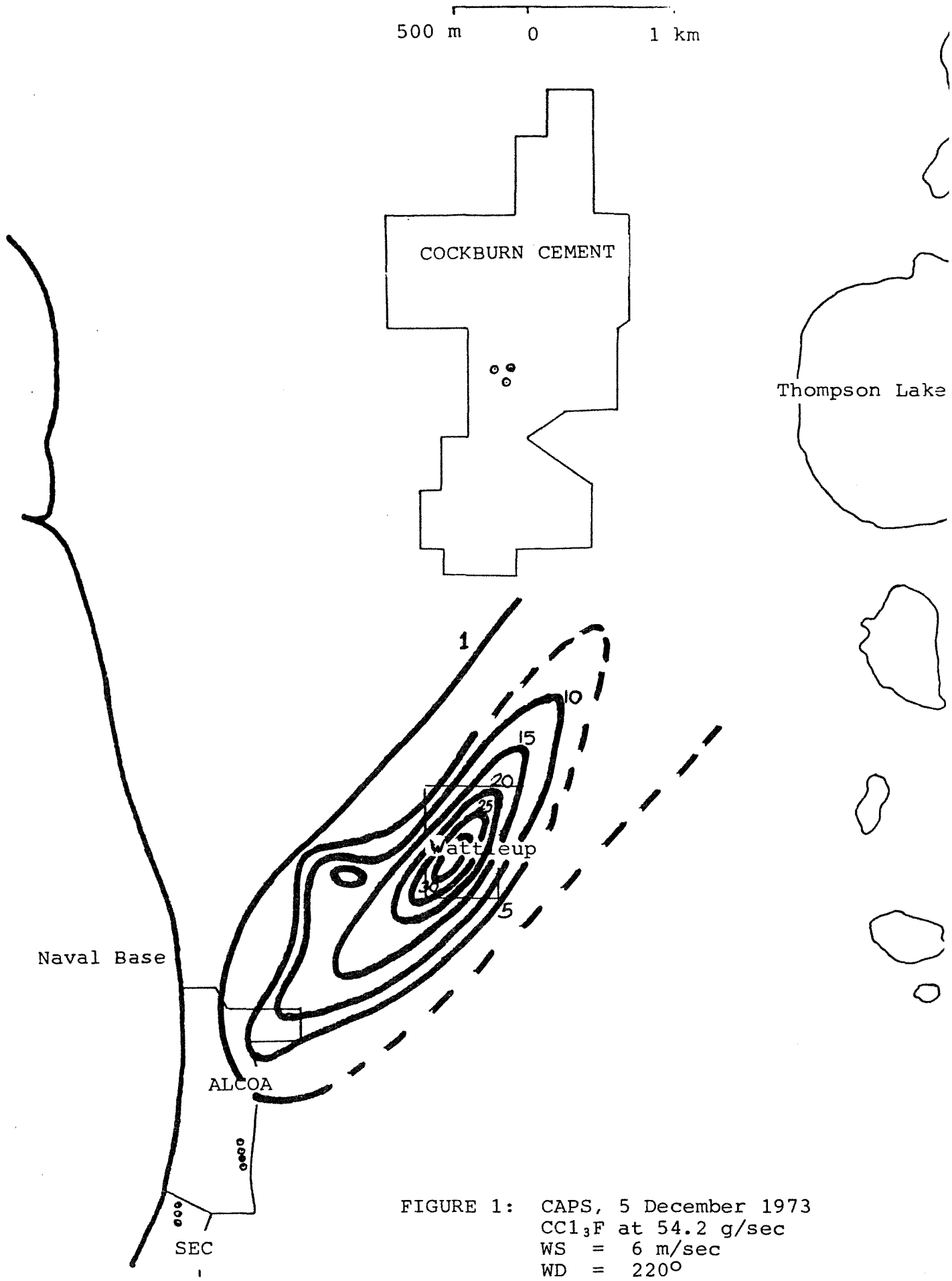

FIGURE 1: CAPS, 5 December 1973
$CC1_3F$ at 54.2 g/sec
WS = 6 m/sec
WD = 220°

The sampling grid for CAPS was designed to obtain maximum information over the vacant land immediately north of Alcoa. Consequently data over Wattleup are sparse and the contouring to the east of the plume centreline is somewhat speculative. The following observations are made:

3.1 When compared with KAMS 1 and 2 no spurious Freon 11 sources are evident probably because of lack of data to the east of the plume centreline. No SF_6 was released so control from this source was absent.

3.2 The plume "comes to ground" quite quickly with a rapid drop off in ground level concentration, although again data are lacking to the north east.

3.3 The highest concentrations fall on the Wattleup Townsite.

3.4 A distinct "topographical affect" can be seen with relatively high concentrations on the hilly terrain before Mount Brown and in its lee. This effect was predicted from theory and earlier tests using smoke flares. In the case of CAPS the lee eddy (or rotor) appears to be very close to Mt. Brown.

4. KAMS 1

In KAMS 1 Freon 11 was released at a rate of 25.3 g/sec and SF_6 at 19.6 g/sec. The wind speed was 6 m/sec and the wind direction 220°. Contours for Freon 11 are shown in Figure 2 and those for SF_6 in Figure 3. The following observations are made:

4.1 The plume again has come to ground quickly with the ground level concentrations falling off rapidly to the north east.

4.2 The highest concentrations of both tracers fall on the Wattleup Townsite.

4.3 Comparison of the SF_6 and Freon 11 contours clearly shows the effect of tracer release from the power station stack. The SF_6 contours originate solely from the stack release. The Freon 11 contours also show the effect of the stack release but in addition show two possible "urban" sources to the east of the centreline. A third possible spurious source (Alcoa?) is indicated by higher Freon 11 values west of the centreline.

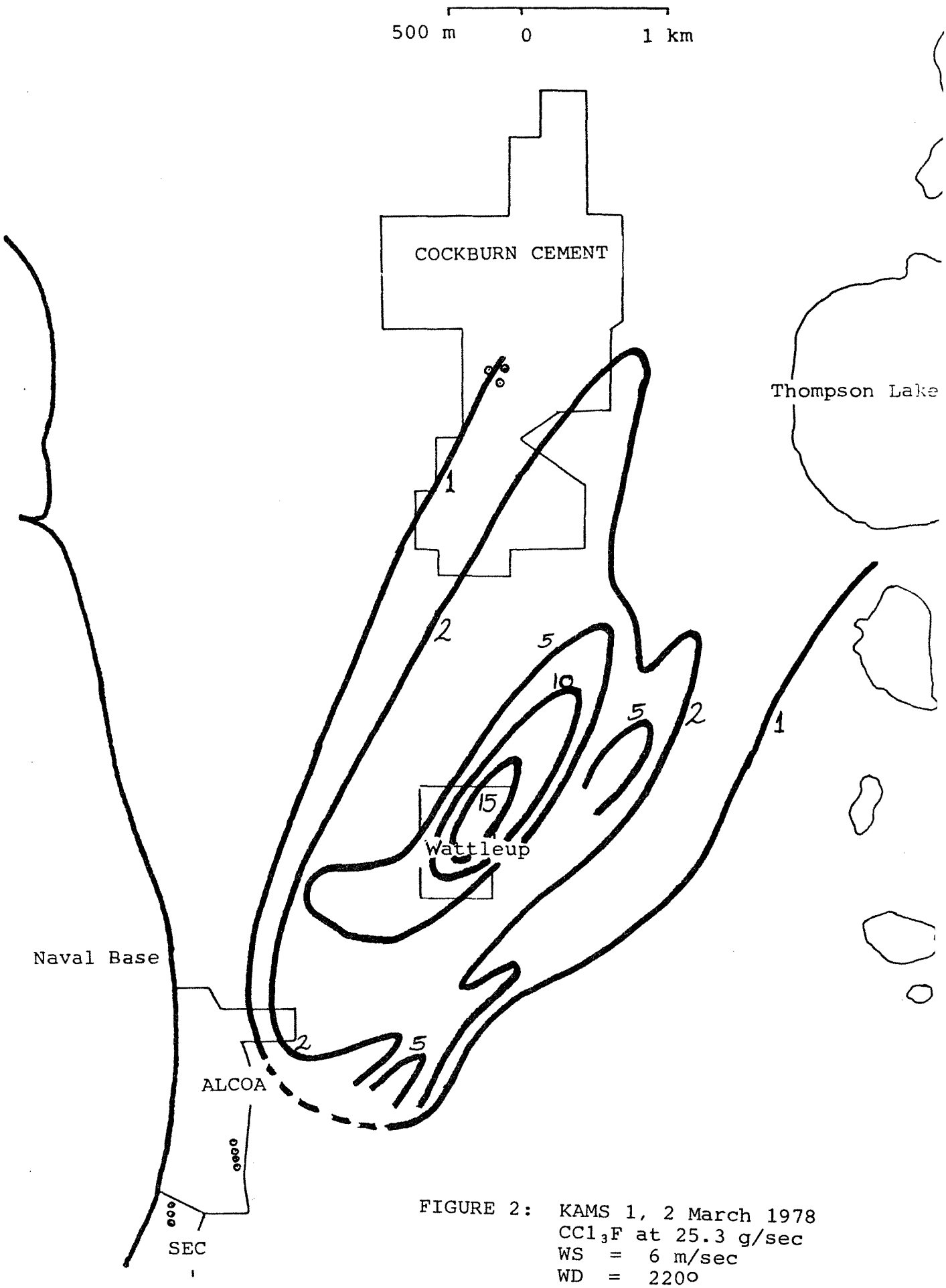

FIGURE 2: KAMS 1, 2 March 1978
CCl_3F at 25.3 g/sec
WS = 6 m/sec
WD = 220o
HMIX = 250 m

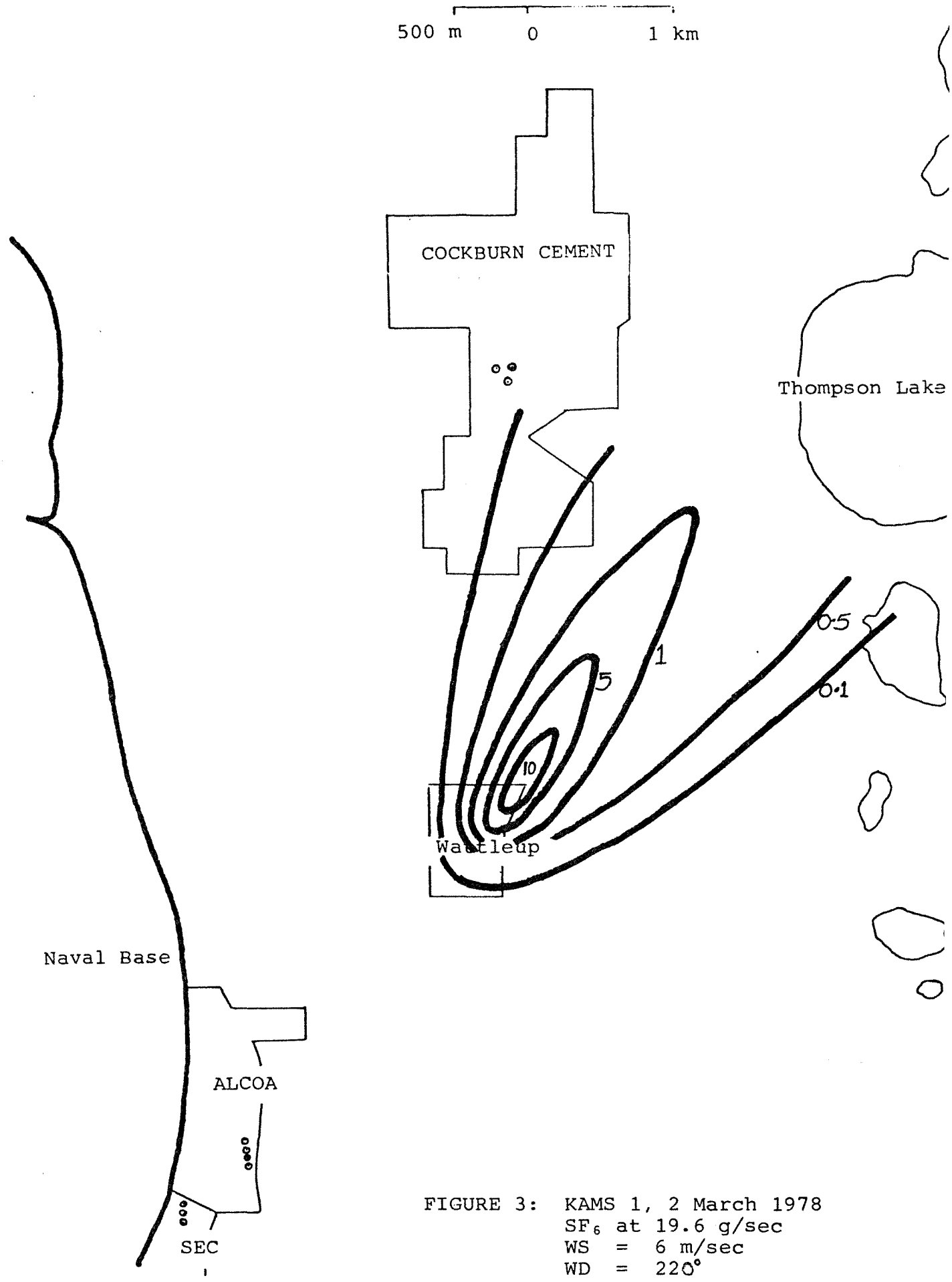

FIGURE 3: KAMS 1, 2 March 1978
SF_6 at 19.6 g/sec
WS = 6 m/sec
WD = 220°
HMIX = 250 m

4.4 KAMS 1 complements CAPS as the highest sampling densities cover adjacent areas. In CAPS the largest number of sampling sites were to the west of the 220° centreline while in KAMS 1 they were to the east. Thus, a "topographic" effect was seen in CAPS but is absent in KAMS 1 while KAMS 1 shows evidence for "urban plumes" which are not seen in CAPS.

5. KAMS 2

For KAMS 2, the Freon release rate was 85.1 g/sec and that for SF_6 29.7 g/sec. The wind speed was 10 m/sec and wind direction 210°. Contours for Freon 11 are shown in Figure 4 and those for SF_6 in Figure 5. The following observations can be made:

5.1 KAMS 2 is quite different from KAMS 1 and CAPS with maximum concentrations for Freon 11 and SF_6 occurring some 3 kilometres further to the north east. Certainly the wind speed is greater in KAMS 2, as is the height of the sea breeze boundary (250 m vs. 425 m).

5.2 In KAMS 2 ground level dispersion of the tracers is much greater, indicating greater mixing in the horizontal.

5.3 A particular feature of interest is the high level of Freon 11 and SF_6 observed at the Wattleup Townsite, quite distinct from the main fallout to the north east. This localised concentration can be attributed to the "topographic effect" of Mt. Brown, although it appears in KAMS 2 that the eddy has moved further downwind. Unfortunately no data is available between Mt. Brown and the SEC to show if higher concentrations observed in CAPS occur in KAMS 2.

5.4 An "urban plume" identical to one in KAMS 1 can be seen in the KAMS 2 contours. The second KAMS 1 "urban plume" is not observable in KAMS 2 because of lack of data.

6. CONCLUSIONS

6.1 Tracers are valuable adjuncts to mathematical modelling in defining plume behaviour. In particular, they can resolve non classical features of dispersion. In the case of CAPS and KAMS 1 and 2 the tracers clearly show topographic effects.

6.2 Sulphur hexafluoride is the preferred tracer as background levels are undetectable. Freon 11 being much less expensive can be used but background levels must be taken into account.

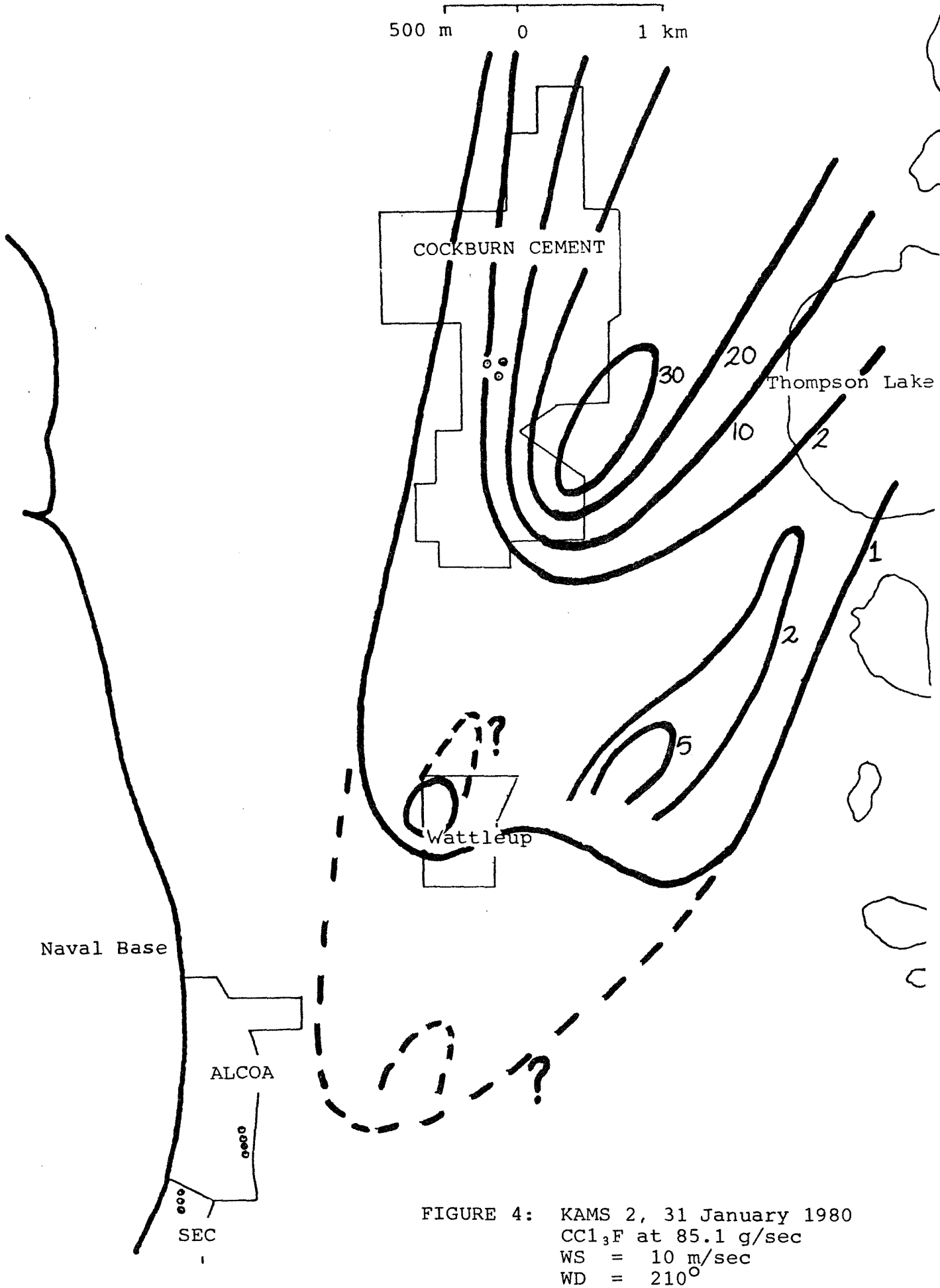

FIGURE 4: KAMS 2, 31 January 1980
CCl_3F at 85.1 g/sec
WS = 10 m/sec
WD = 210°
HMIX = 425 m

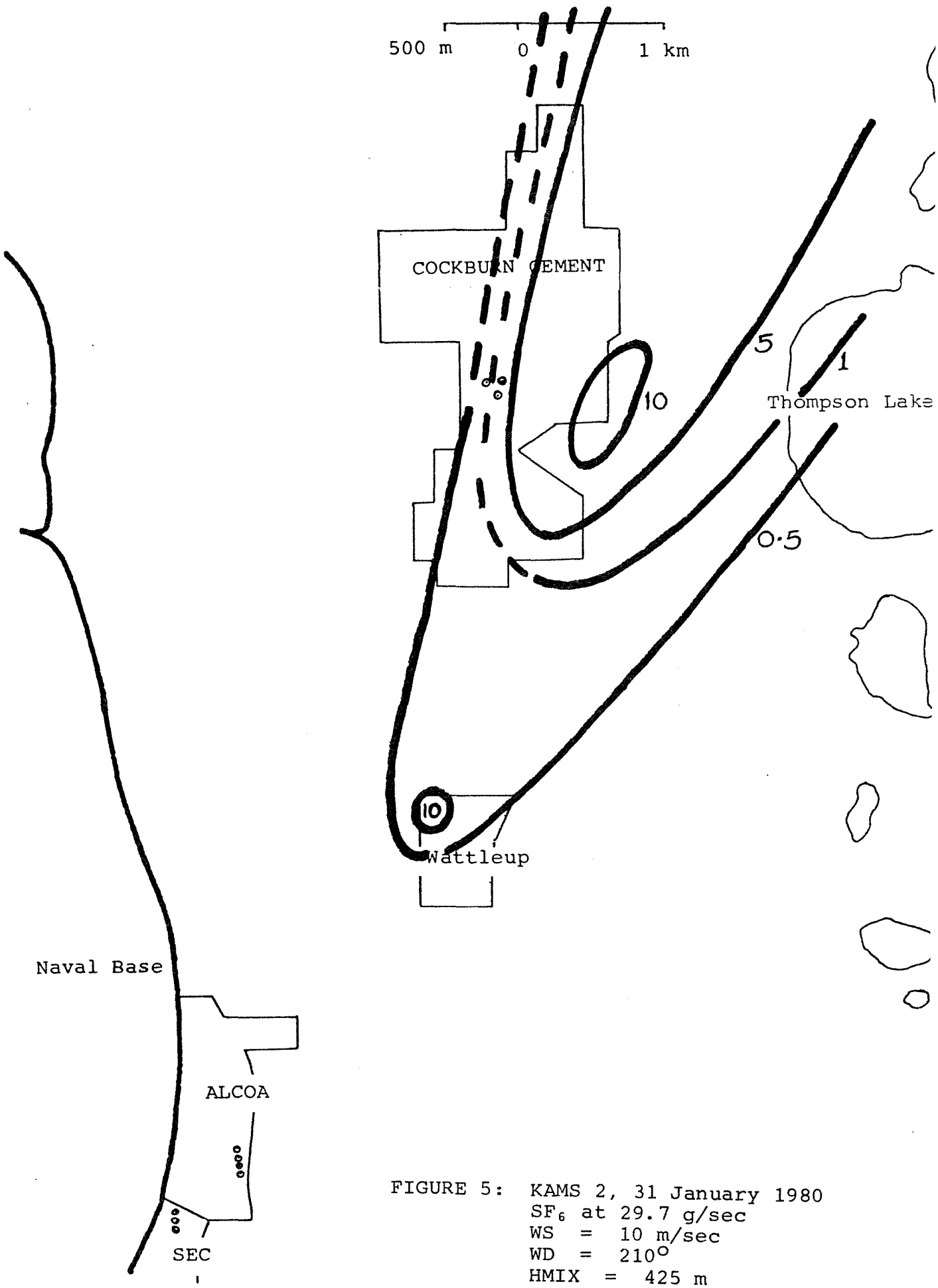

FIGURE 5: KAMS 2, 31 January 1980
SF_6 at 29.7 g/sec
WS = 10 m/sec
WD = 210°
HMIX = 425 m

6.3 SF_6 and Freon 11 when released together can provide useful cross checks. Alternatively the two tracers could be released from separate sources to give an idea of relative contributions to ground level concentrations. In this latter case extensive background measurements of Freon 11 should be taken to validate the data.

NOTES ON PLUME RISE AND GAUSSIAN DISPERSION CALCULATIONS FOR THE JANUARY 31, 1980 TRACER EXPERIMENT

K. RAYNER AND V. PAPARO

1. INTRODUCTION

Meteorological and dispersion data collected during the January 31, 1980 tracer experiment permit a variety of analyses to be performed and will facilitate the testing of dispersion models developed in KAMS. At this stage, a preliminary analysis of the application of plume rise and Gaussian dispersion calculations has been completed, as described below.

2. PLUME RISE

A numerical plume rise model was run for this experiment using emissions data provided by the SEC and the best available atmospheric data. The model obtains a numerical solution to the equations of continuity, momentum and heat (for further details see Rayner (1974)).

Unfortunately the coastal radiosonde releases during the experiment were not successful and hence no reliable vertical profiles of temperature or wind velocity were available in the region of initial plume rise. For the purpose of analysis, two model runs were carried out using different assumed vertical temperature profiles. Figure 1 is a plot of the plume centreline for a temperature profile and wind profile determined from the inland radiosonde release. The sea breeze interface can be seen between 300 and 415 metres height on the temperature plot. Also shown is the shape of the Gaussian cross section assumed by the model. The centreline and cross section may be compared over the first kilometre, with the results of plume photography from the experiment, plotted in Figure 1 as the shaded region. Although the downwind distance is relatively small (limited by visual interpretation of photographs) the agreement between calculated and observed plume trajectories is good. The limiting effect of the interface "lid" on plume rise is clearly seen in this Figure.

Figure 2 shows the model output for a different assumed temperature profile (with all other input data fixed). Here, the temperature profile was constrained to be isothermal, in line with the predictions of a sea breeze model run by Dr. P. Rye (pers. comm.). The resultant plume rise is suppressed by the stable density gradient. Comparison with the photographed plume, although inconclusive, suggests the stability effect is too severe (i.e. the atmosphere was actually less stable than isothermal).

The Plume rise model has performed well in three tests to this time (Pinjarra (1975), Kwinana (1978), Kwinana (1980)) and hence may be applied in the future with some confidence.

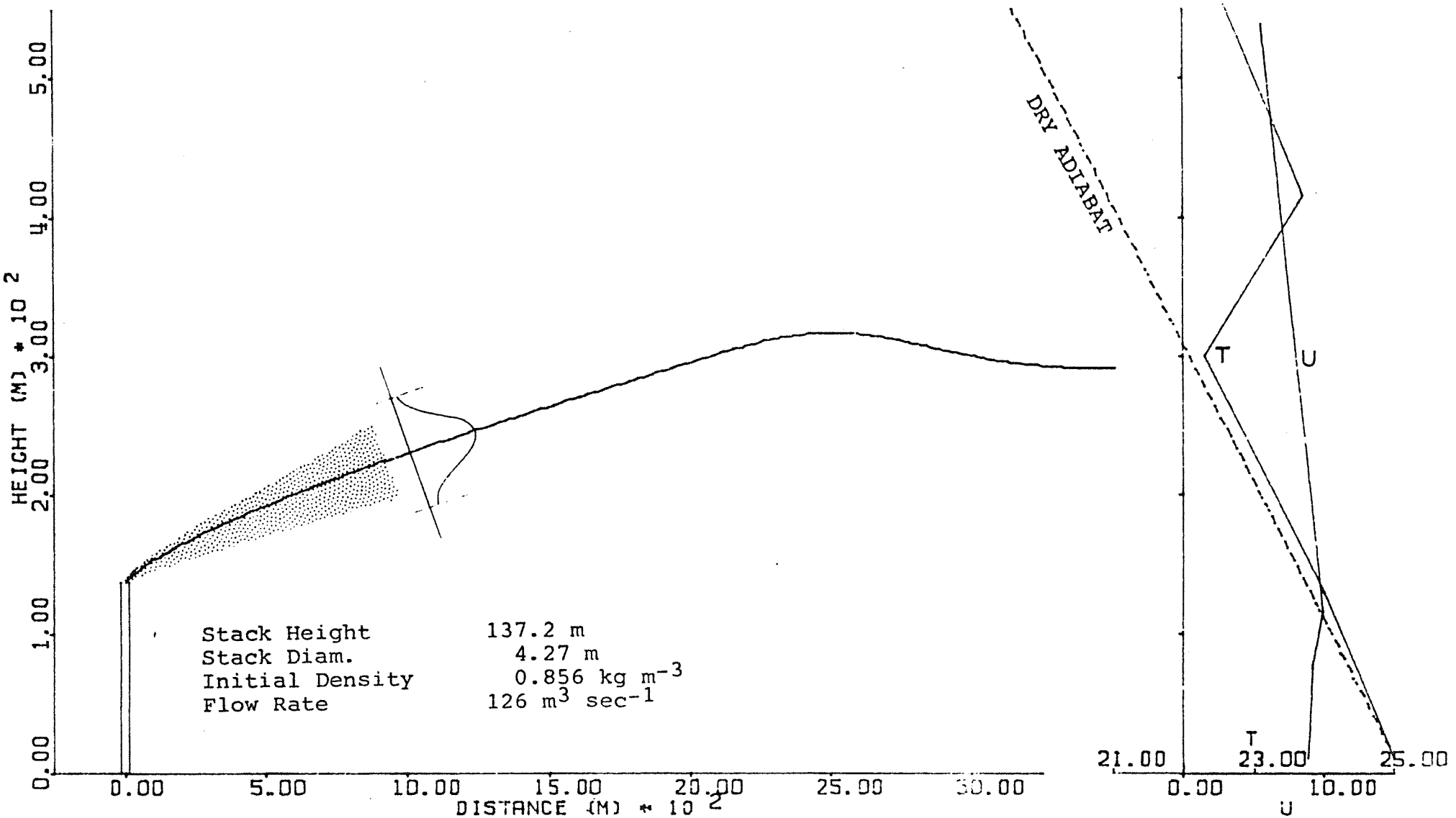

Figure 1 Plume Rise - temperature profile from inland sonde.

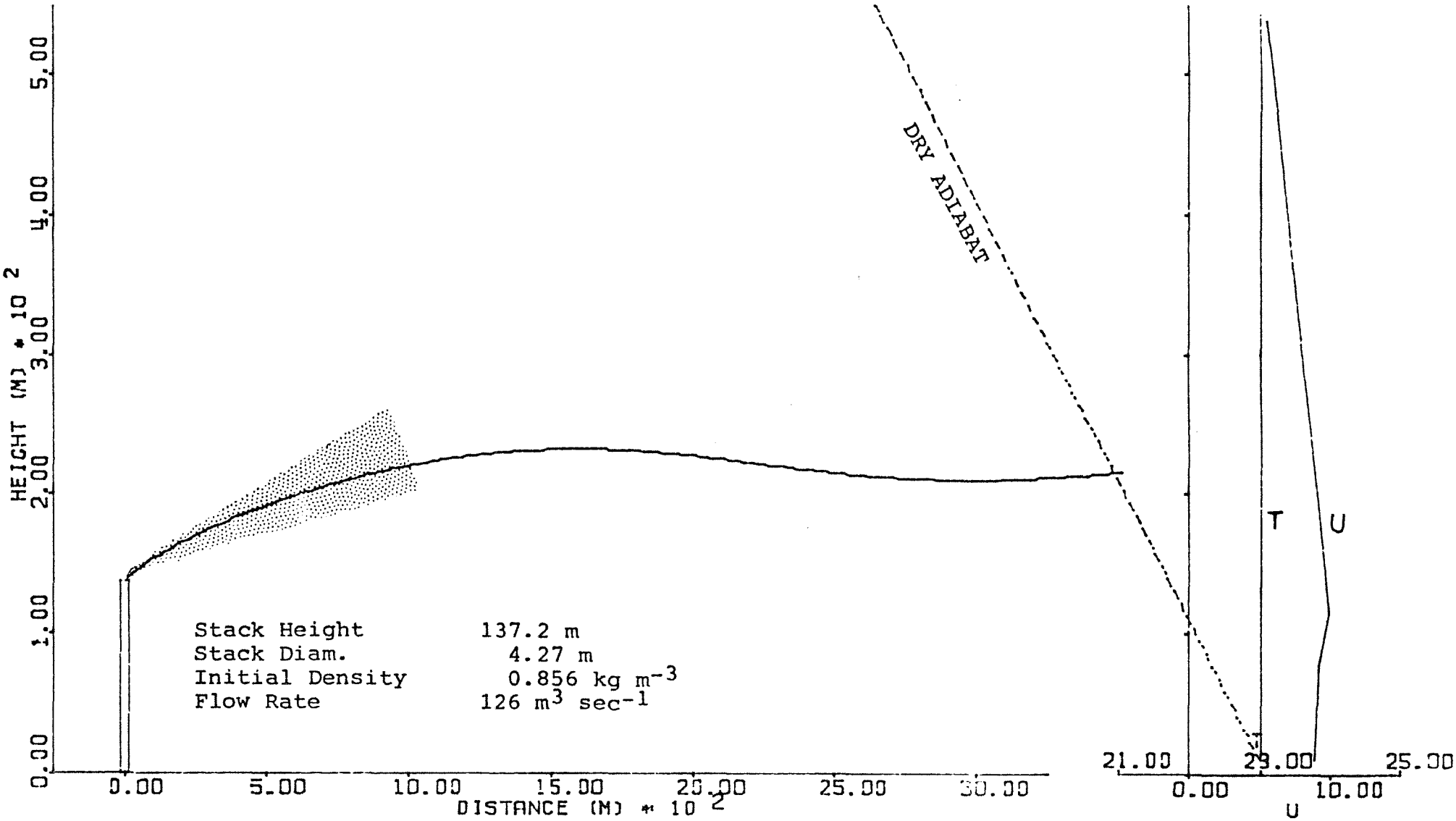

Figure 2 Plume Rise - temperature profile isothermal.

3. GAUSSIAN DISPERSION

For describing short to medium range diffusion, the Gaussian plume approach is probably more applicable than other approaches (e.g. eddy diffusivity), and further, is easy to use. The major drawback with this method is the requirement to specify the plume dimensions (σ_y and σ_z) as a function of both downwind distance and atmospheric stability. Procedures for this have been proposed for the unstable case (Willis and Deardorff (1974)), requiring continuous estimates of the surface heat and momentum fluxes. In the absence of these estimates, it is customary to classify stability into categories (Turner 1970). The following calculations show this method to be unacceptably coarse.

The distribution of SF_6 measured during the tracer experiment is plotted as contours in Figure 3. The Gaussian formula described by Paparo and Rayner (1978) was used to simulate the dispersion of tracer gas. Estimates of surface layer stability from the Hope Valley Base Station are consistent with choosing Stability Class B. As can be seen in Figure 4 however, the predicted maximum G.L.C. occurs much too close to the release point, indicating an overestimation of instability. Paparo and Rayner found Class C (slightly unstable) gave good predictions for the March 1978 experiment. Figure 5 shows that again the predictions are acceptable, although the maximum level is underpredicted and the dual maxima points (see Figure 3) cannot be simulated. However, there is no sound criteria for choosing C! In fact, if the stability of the marine air flowing over the coast is considered, Class D (slightly stable would be chosen. Figure 6 shows that calculations for Class D produce no significant concentrations in the region of interest (i.e. the maximum is moved far downstream).

Two conclusions may be drawn from the above. Firstly, if stability categories are to be used, the criteria for choosing them must be tightened to avoid any ambiguity. Secondly, even if the criteria are rigid, transition from one Class to another, as must occur throughout the day, leads to catastrophic changes in predicted ground level distribution for medium to strong winds. It is not reasonable to expect such discontinuities to be correctly smoothed for long term simulations; bias in Class selection will still be reflected in the results.

It is evident therefore that significant effort must be directed towards the valuation of σ_y and σ_z as continuous functions of measured variables (e.g. $\sigma\theta$, Monin-Obukhov length) if Gaussian plumes are to be considered.

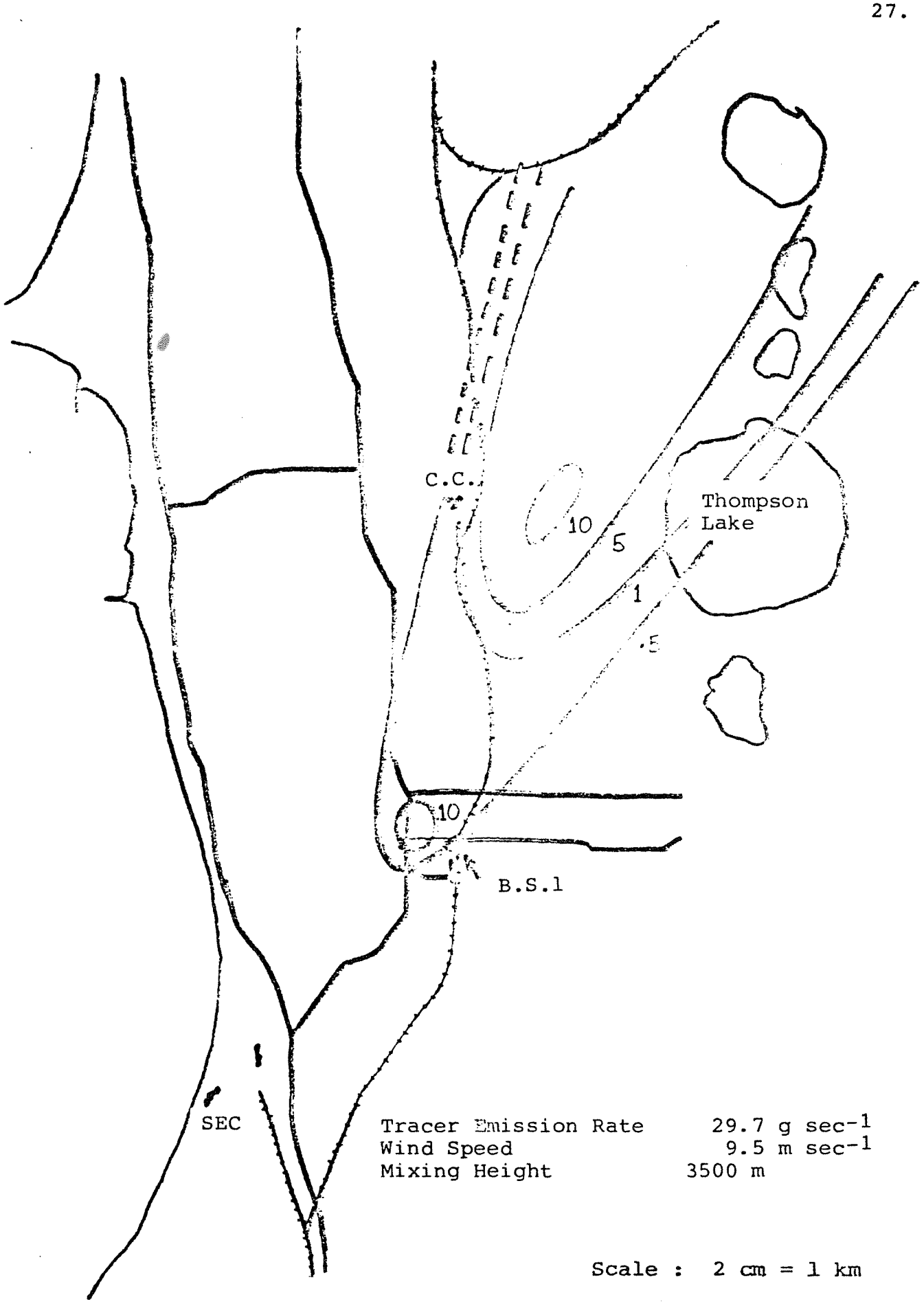

Figure 3 Contours of measured SF_6 concentrations

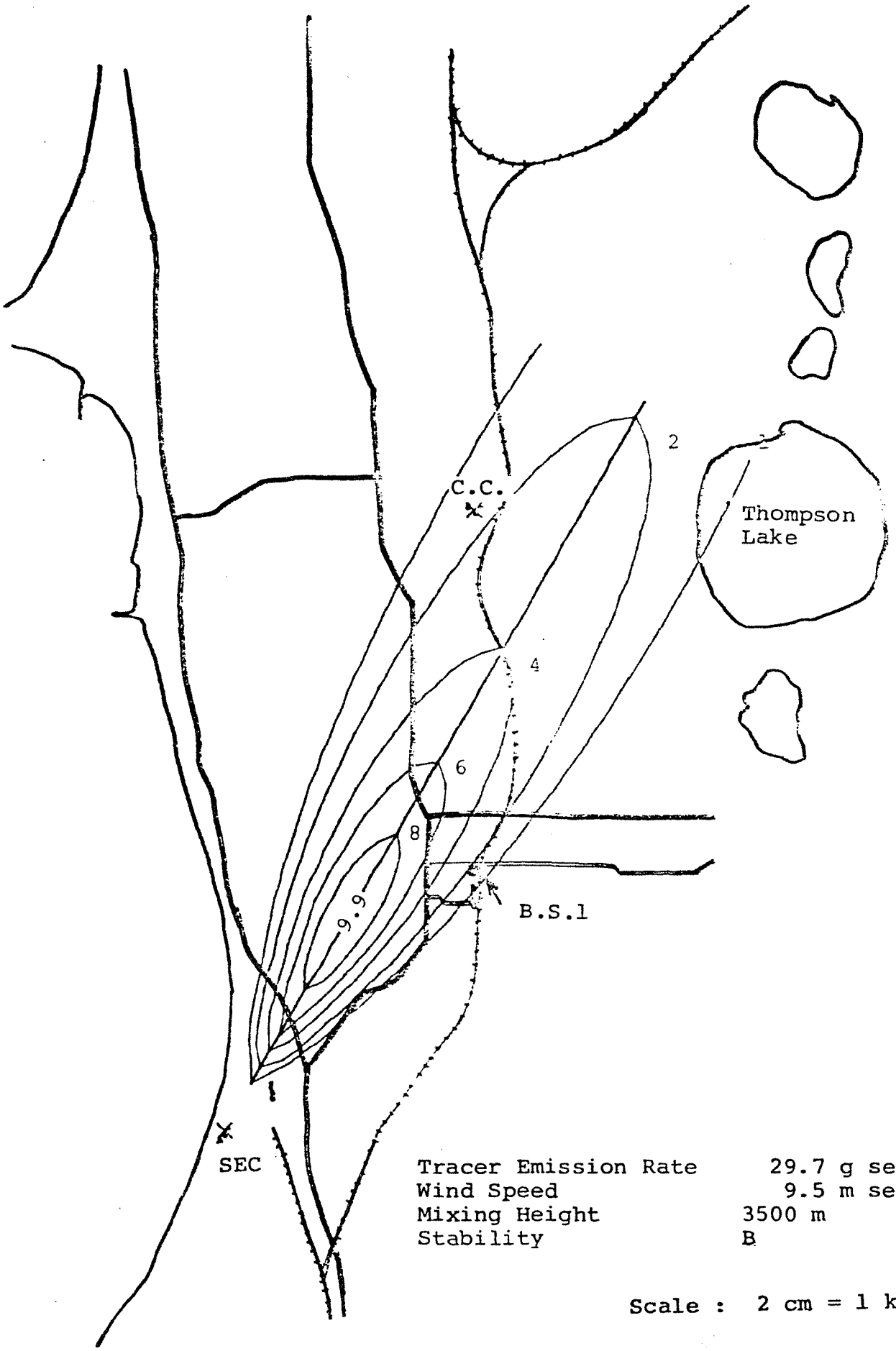

Figure 4 Predicted G.L.C. Contours - Stability Class B

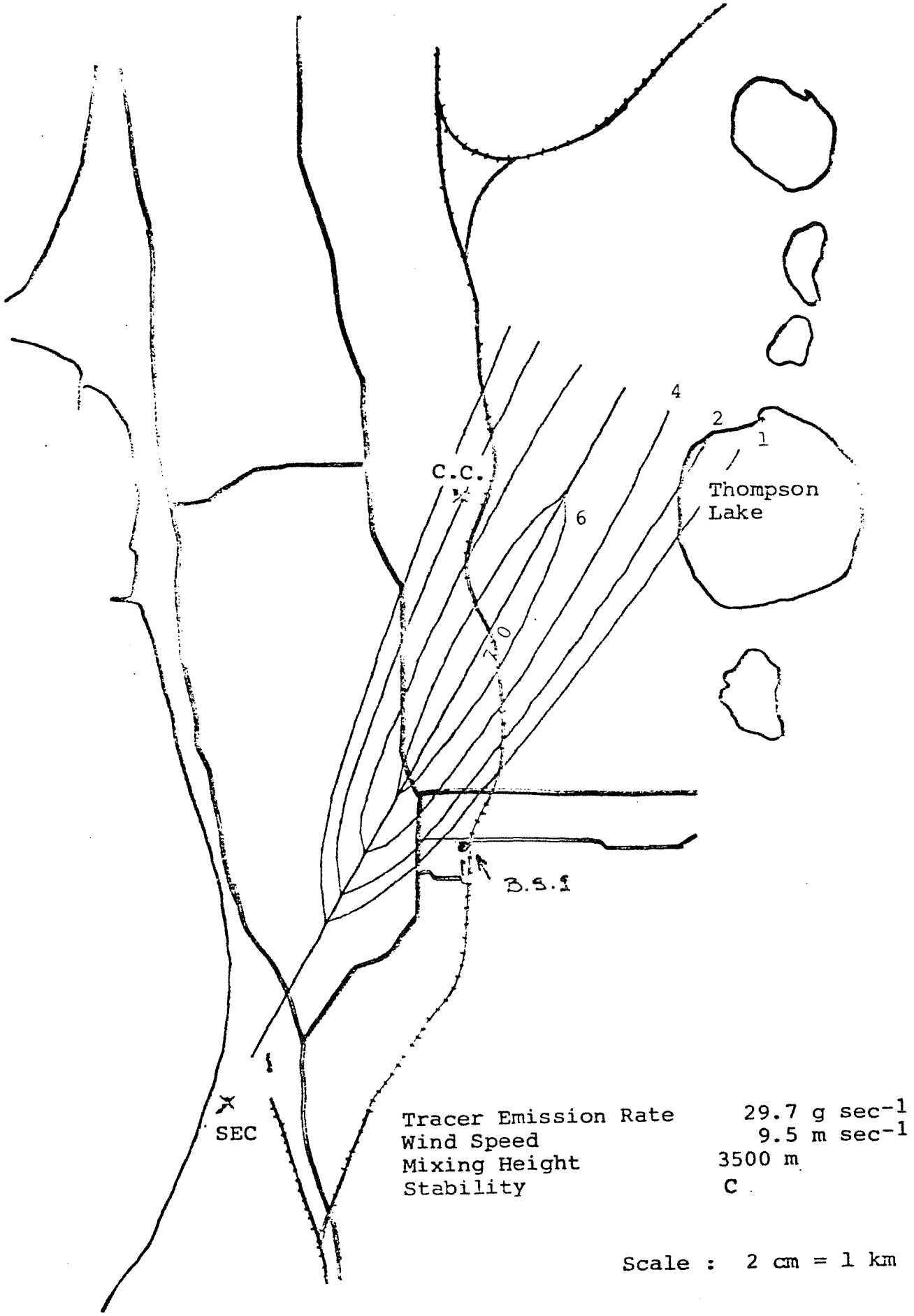

Figure 5 Predicted G.L.C. Contours - Stability Class C

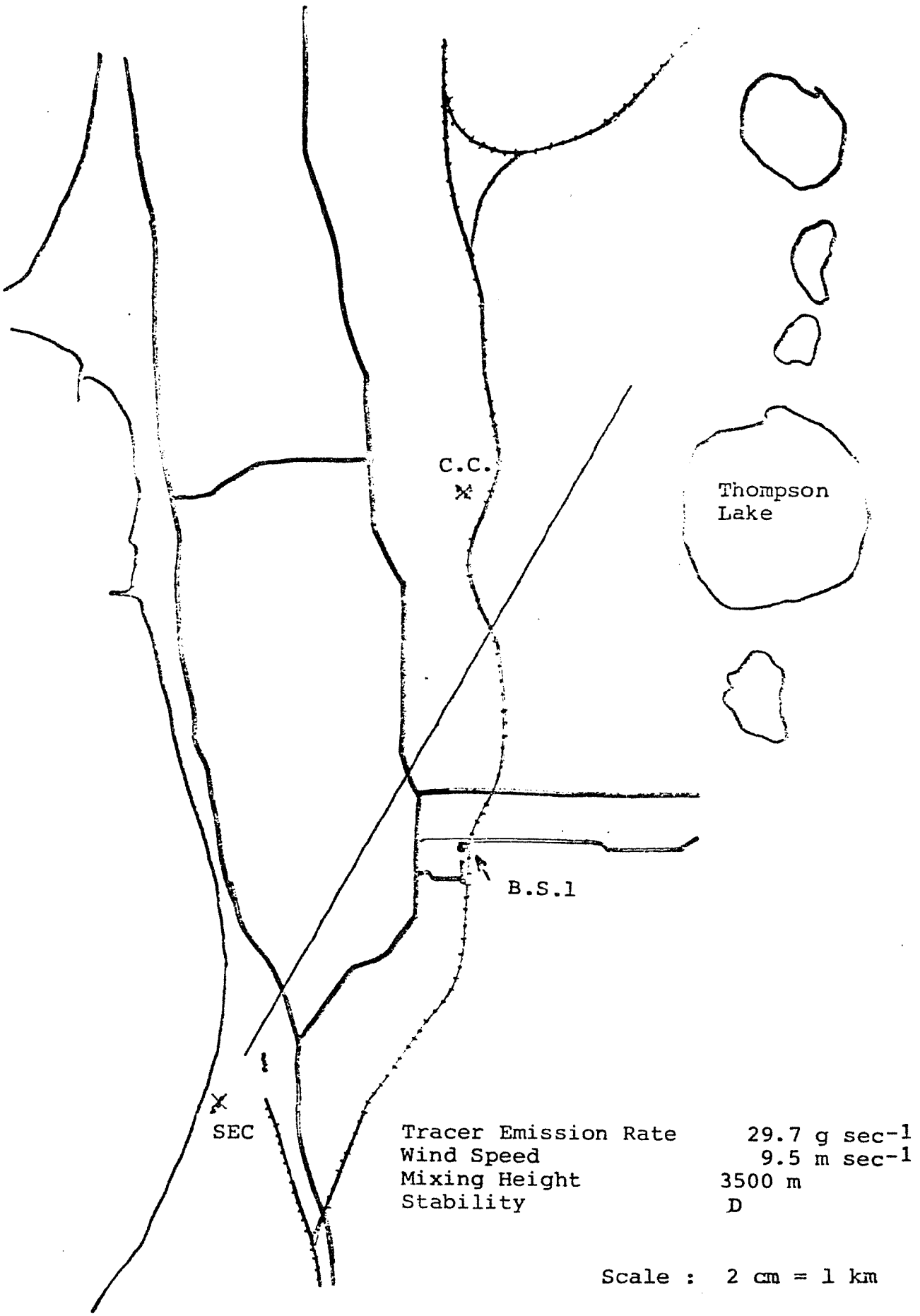

Figure 6 Predicted G.L.C. Contours - Stability Class D

4. INTERNAL BOUNDARY LAYERS

The development of an internal boundary layer as the sea breeze flows from the water over the land is obviously an important phenomena to be considered in dispersion calculations. The destabilizing effect of ground surface heating will be restricted to this boundary layer. As the layer grows it will interact with plumes from elevated sources causing rapid mixing of the pollutant some distance downwind of the source. Dr. P. Rye (pers. comm.) has incorporated this effect in an eddy diffusion model. Alternatively, a Gaussian puff model could also be modified to incorporate the effect, as shown in the schematic of Figure 7. The rate of growth of σ_y or σ_z (i.e. $\frac{d\sigma_y}{dx}$ or $\frac{d\sigma_z}{dx}$) will marked increase as the plume intersects the growing boundary layer.

Appendix I contains a schematic and an equation set for describing the growth of the internal boundary layer. This model, similar to that proposed by Venkatram (1977), applies the mixing layer theory of Rayner (1980) in a Lagrangian framework to a column of air. Given the surface heat flux $\hat{H}$, the friction velocity U_* and the vertical temperature gradient $d\theta/dz$, a solution of the layer growth may be obtained. The model will be implemented in due course.

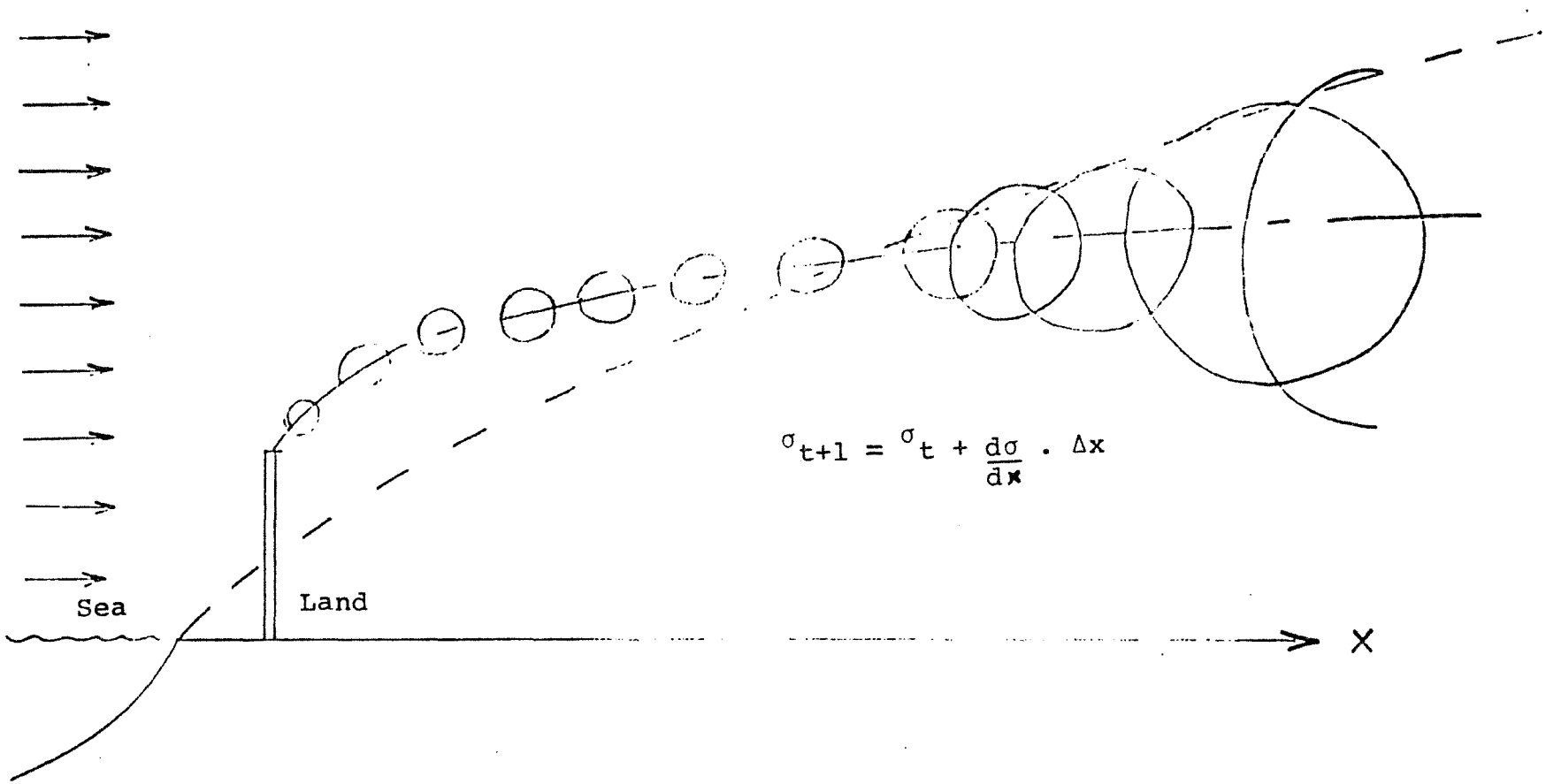

Figure 7 Gaussian Puff Model with Developing Internal Boundary Layer

APPENDIX I

INTERNAL BOUNDARY LAYER

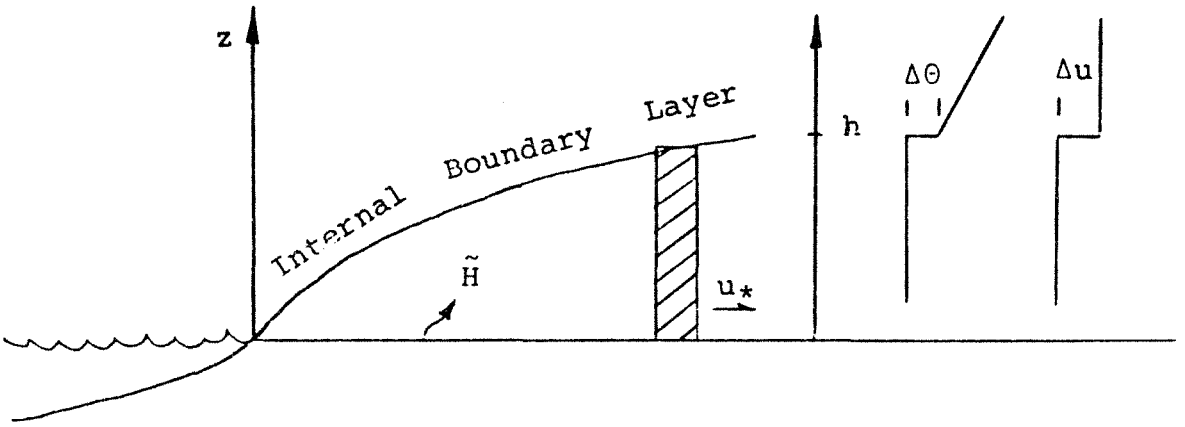

$$h \frac{dE_S}{dt} = q_*^3 - (C_F + C_E) E_S^{3/2} \qquad (1)$$

$$\frac{dh}{dt}\left[E_S + \frac{gh\Delta\Theta}{To} - C_S \Delta U^2\right] = C_F E_S^{3/2} \qquad (2)$$

with $E_S = \frac{1}{h}\int_o^h \bar{E}\, dz$, $\bar{E} = \sigma u_2 + \sigma v_2 + \sigma w_2$

$$q_*^3 = w_*^3 + \eta^3 u_*^3 \quad , \quad w_*^3 = \frac{g\tilde{H}h}{\rho C_p to}$$

Coefficients: $C_F = 0.25$, $C_S = 0.20$

$C_F = 1.15$, $\eta = 1.33$

For steady convective conditions $\begin{pmatrix}\Delta T \text{ large} \\ \Delta U \text{ small}\end{pmatrix}$

$$\frac{gh\Delta\epsilon}{To} \frac{dh}{dt} = \kappa_A w_*^3 \quad , \quad \kappa_A = \frac{CF}{C_F + C_E} \simeq 0.2$$

MIXING DEPTHS AT KWINANA, 31ST JANUARY 1980

1. Analysis of Radiosonde Measurements

P.J. Rye

INTRODUCTION

In contrast to the sea breeze observed during the last successful intensive study, on 2nd March 1978, the one on this day represented the 'upper tail' of the distribution of sea breeze strengths observed at Perth. As such, the pollutant dispersal characteristics measured in the intensive study should provide a useful data set for comparison with the earlier results.

While being a relatively typical example of an intense sea breeze, the detailed characteristics showed a feature not typical of the type. Reasons for this feature are detailed below, and its effect on pollution dispersal considered.

OBSERVATIONAL RECORDS

An extensive set of meteorological records was obtained on the study day. In addition, Bureau of Meteorology analyses have been used to interpret changes in the large-scale winds which affect sea breeze development. The data used in the present analysis were:

(a) Five pilot balloon releases, at 1255, 1335, 1425, 1500 and 1535 W.S.T., all but the first providing temperature soundings. The data from these ascents is summarised in figures 1 to 6.

(b) Surface analyses at 0600, 0900, 1200 and 1500 W.S.T.

c) Wind speeds and directions analysed at 10-minute intervals, from the Wattleup and Hope Valley 10-metre anemometers.

SUMMARY OF ANALYSES

(a) Radiosonde Data

To be consistent with the well-developed speed of the sea breeze, it could be expected that the depth of the inflow would be large. This was so for the 1255 ascent, with strong inflow below 400 m , and (in the probable absence of any strong inversion) a gradual weakening above until offshore flow was encountered at about 700 m. (see fig. 1).

By contrast, the inflow depth at 1335 had decreased to about 300 m. At this time, there was no evidence of an inversion (fig. 1), and the reversed vertical shear (fig. 2) was consistent with significant offshore stress on the sea breeze inflow. The temporary reduction of wind speed from about 9 ms^{-1} to 7.5 ms^{-1} is evident not only in fig. 1, but also in the base station traces (fig. 3).

From the 1425 sounding onward, the sea breeze appears to have largely 'recovered', returning to speeds of 9-10 ms^{-1}, and with a strong inversion evident. However, the inflow depth shown by this and subsequent soundings did not return to the initial value, remaining at 400-500 m.

(b) The cause of the temporary retardation of the sea breeze at about 1335 is clearly revealed by analysis of the surface pressure fields on the 0600, 0900, 1200 and 1500 surface charts. The north-south pressure gradient was estimate d on a line between Augusta and Jurien Bay, giving the following estimates of the easterly geostrophic wind component:

0600	12.3 ms^{-1}
0900	13.1
1200	15.1
1500	25.7

The 0600 radiosonde released from Perth Airport showed much lower winds, at about 7-8 ms^{-1}. This was moderately consistent with nongeostrophic effects (principally an isallobaric term estimated at 4 ms^{-1} in the morning, decreasing to give a nine-hour average of 2 ms^{-1}, both in a westerly direction).

The increase in offshore winds is shown clearly between 1200 and 1500, and is in qualitative agreement with a measured increase from 4-7 ms^{-1} at 1255 to 6-9 ms^{-1} for later soundings (fig. 1).

To analyse the effect that the changes would have had on mixing depth, both the natural tendency of the flow towards turbulence (measured by the Richardson number, $g(\Delta\theta/\Delta z)/(\Delta \underline{v}/\Delta z)^2$) and the height of rise of thermal plumes were calculated. Normally, the mixing depth is defined using the latter only, but the possibility of the former's being relevant has been previously considered (Rye, 1980).

Figure 4 shows the results of the calculations. The Richardson number possesses considerable "noise", due to otherwise negligible temperature errors, but does show that, at the top of the inflow, a value of at least 2 is always attained. Since the lower limit for stability of laminar flow is about 0.2, the effects of this form of instability (known as Kelvin-Helmholtz instability) may be neglected.

The broken lines show the mixing depths computed assuming adiabatic ascent of convective plumes - the method normally used. It can be seen that, for the critical time of 1335, there is an unacceptably large result.

The continuous lines on figure 4 show mixing depths computed assuming non-adiabatic ascent. In this case, the plume temperatures were assumed to decay hyperbolically (according to a -5/3 power law, after Turner 1973) to that of their environment.

The apparently much more reasonable values resulting from the latter approach should draw attention to the importance of the advection of cold air in the sea breeze flow - in most applications, the vertical uniformity of the boundary layer potential temperature renders the difference between the two values small.

Thus, the following values are suggested for the mixing depths over Alcoa Mudlake F.

1335	410 m
1425	320
1500	450
1535	410

It is notable that, in the 1335 case, the mixing depth exceeded the inflow depth. It would therefore be expected that some loss of pollutants downwind would have been observed at this time.

REFERENCES

Rye, P.J. 1980 "Environmental Applications of a Numerical Sea Breeze Model", Conference on Coastal Meteorology, Los Angeles, January 30 - February 1, 1980.

Turner, J.D. 1973 "Buoyancy Effects in Fluids", Cambridge University Press.

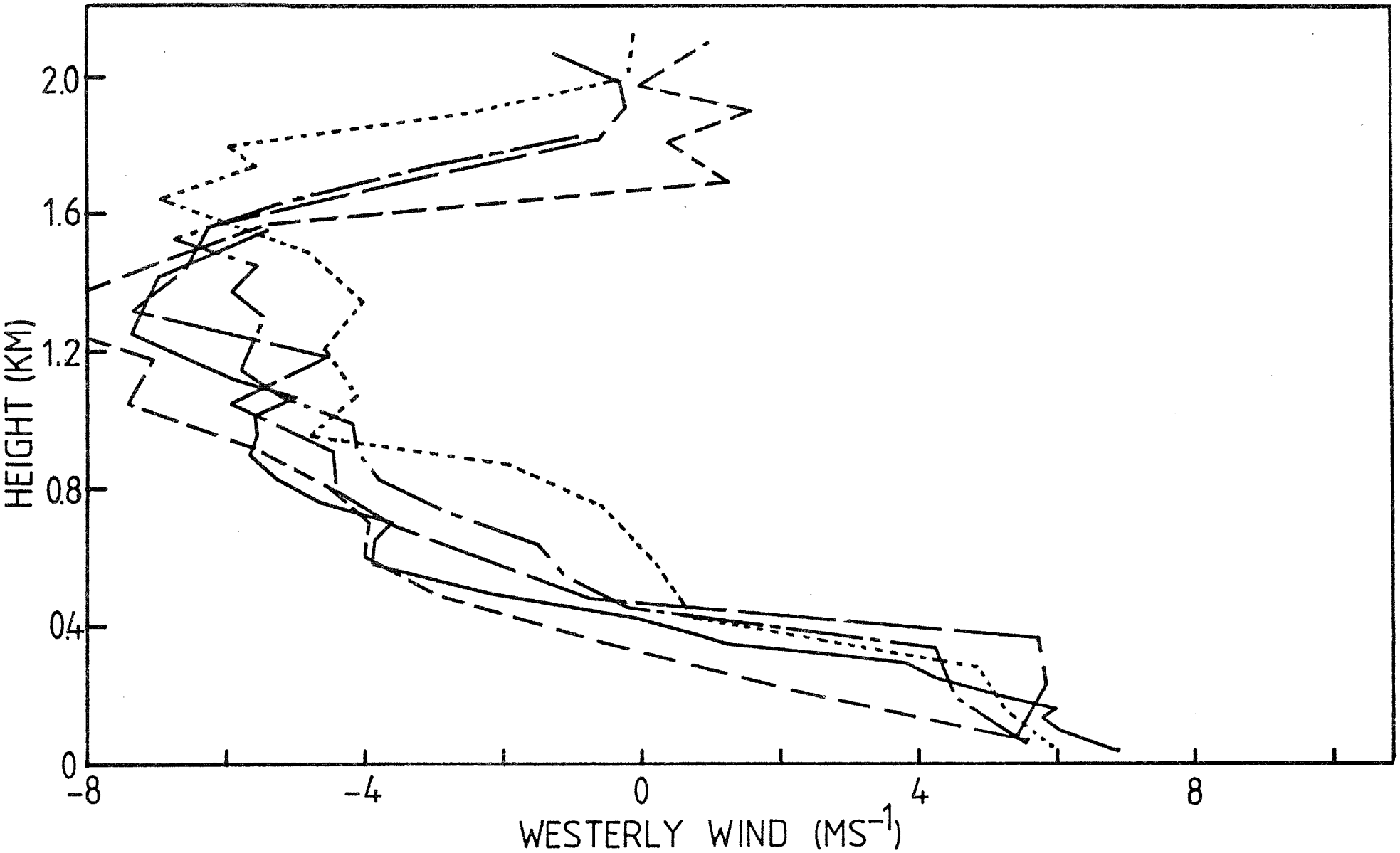

Figure 1: Westerly wind component for each of the five sonde releases at Kwinana on 31st January.

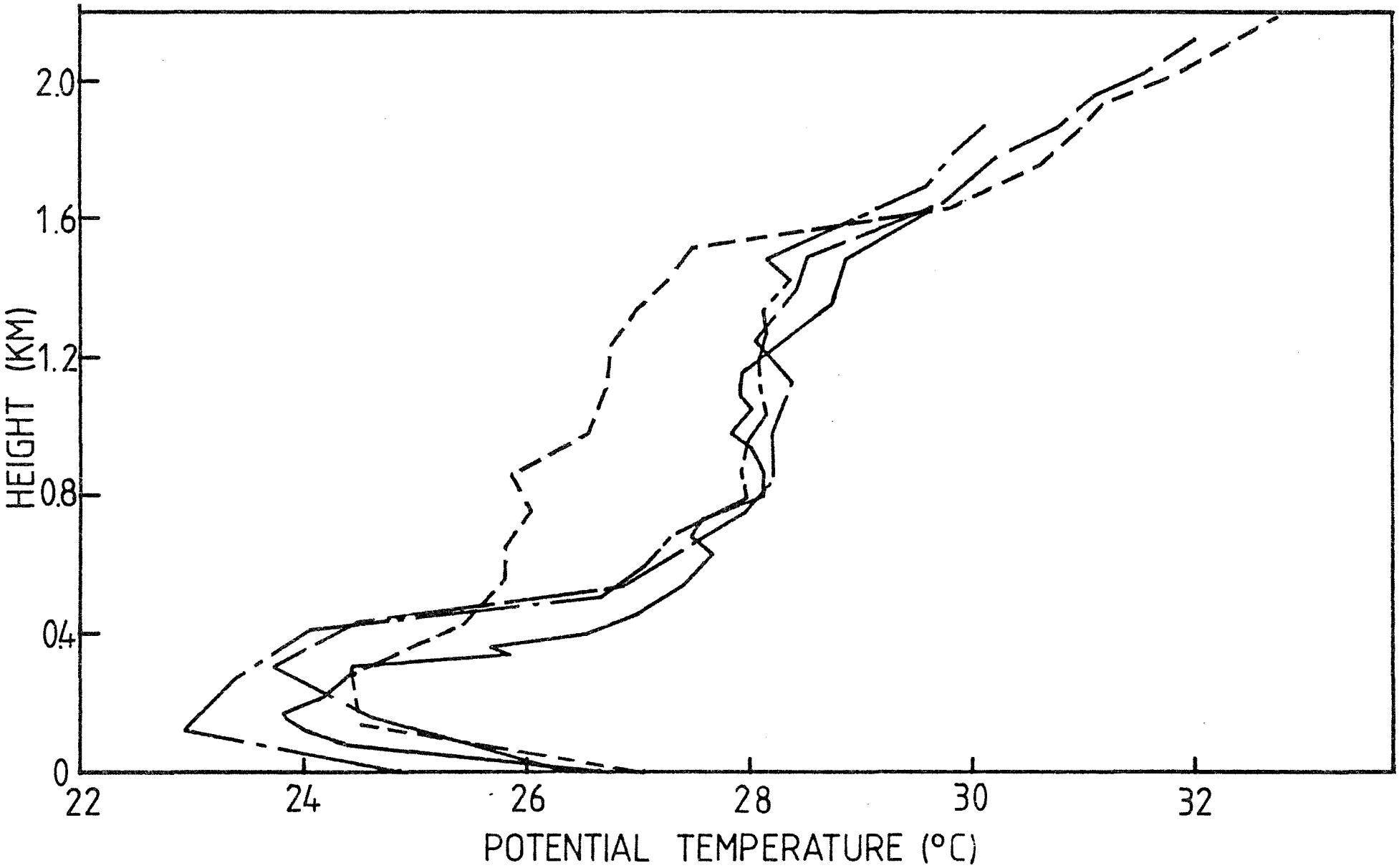

Figure 2: Potential temperatures for all but the first sonde released from Kwinana on 31st January.

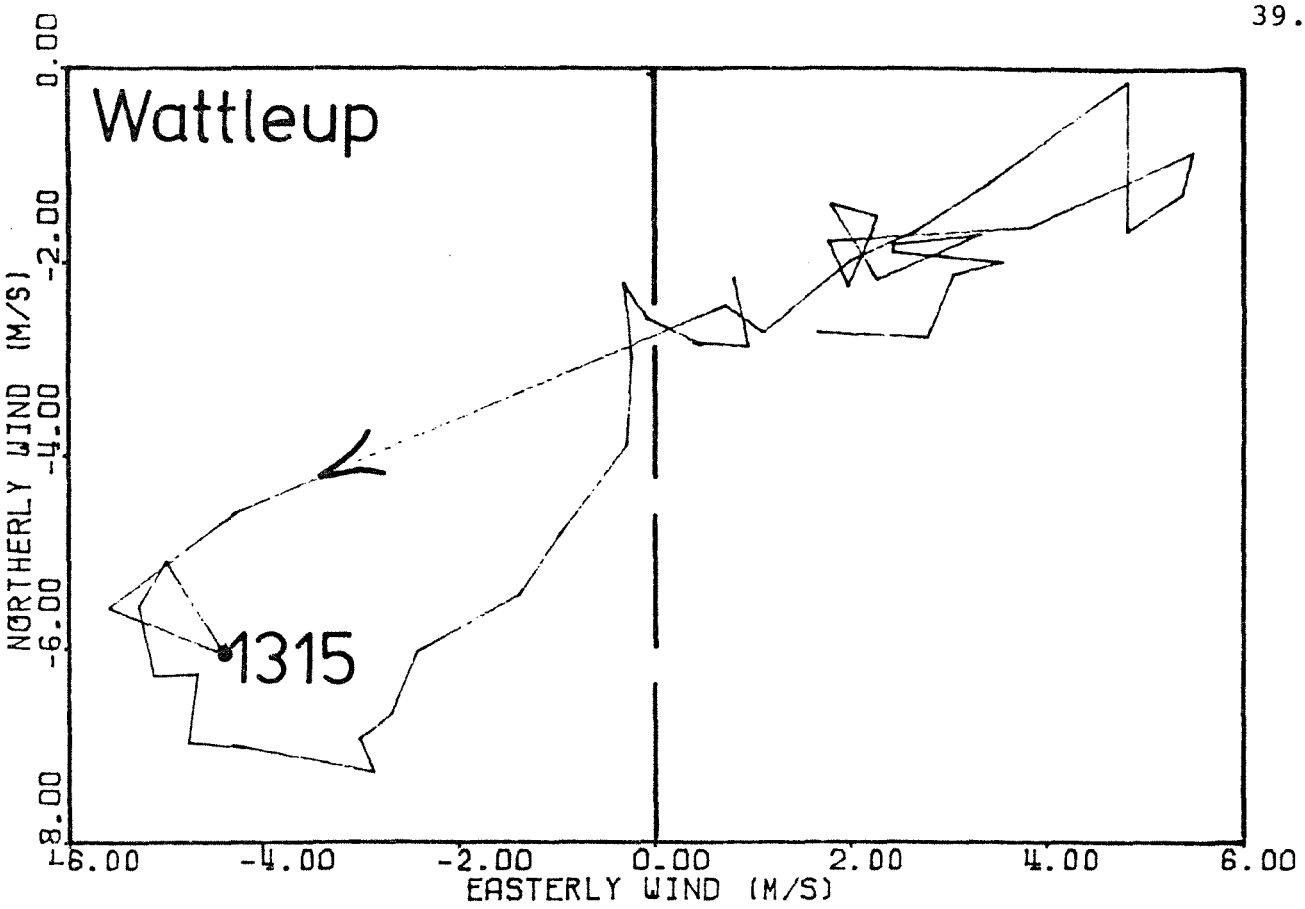

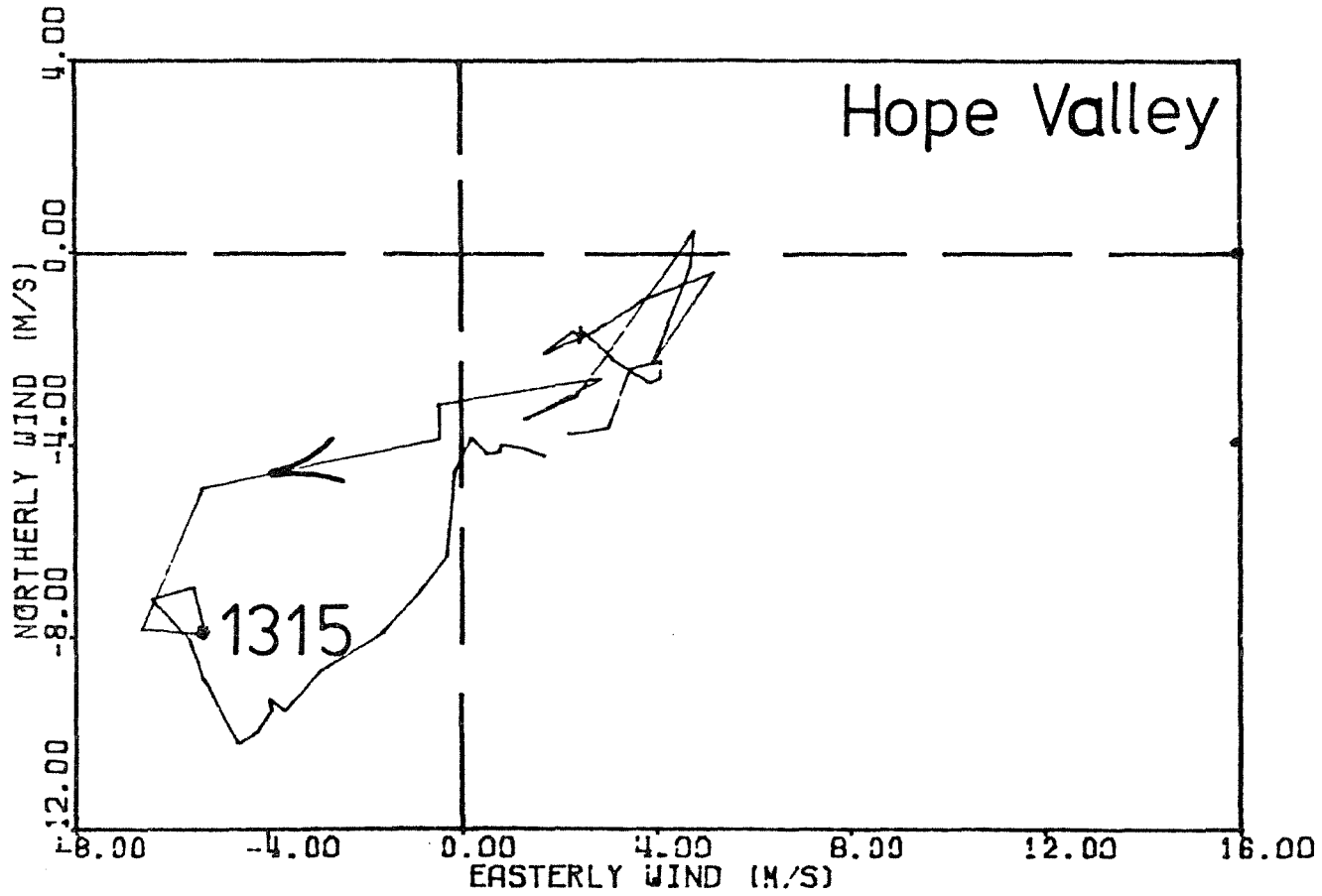

Figure 3: Hodograms for both base stations, showing 10 metre wind variation on 31st January as function of time.

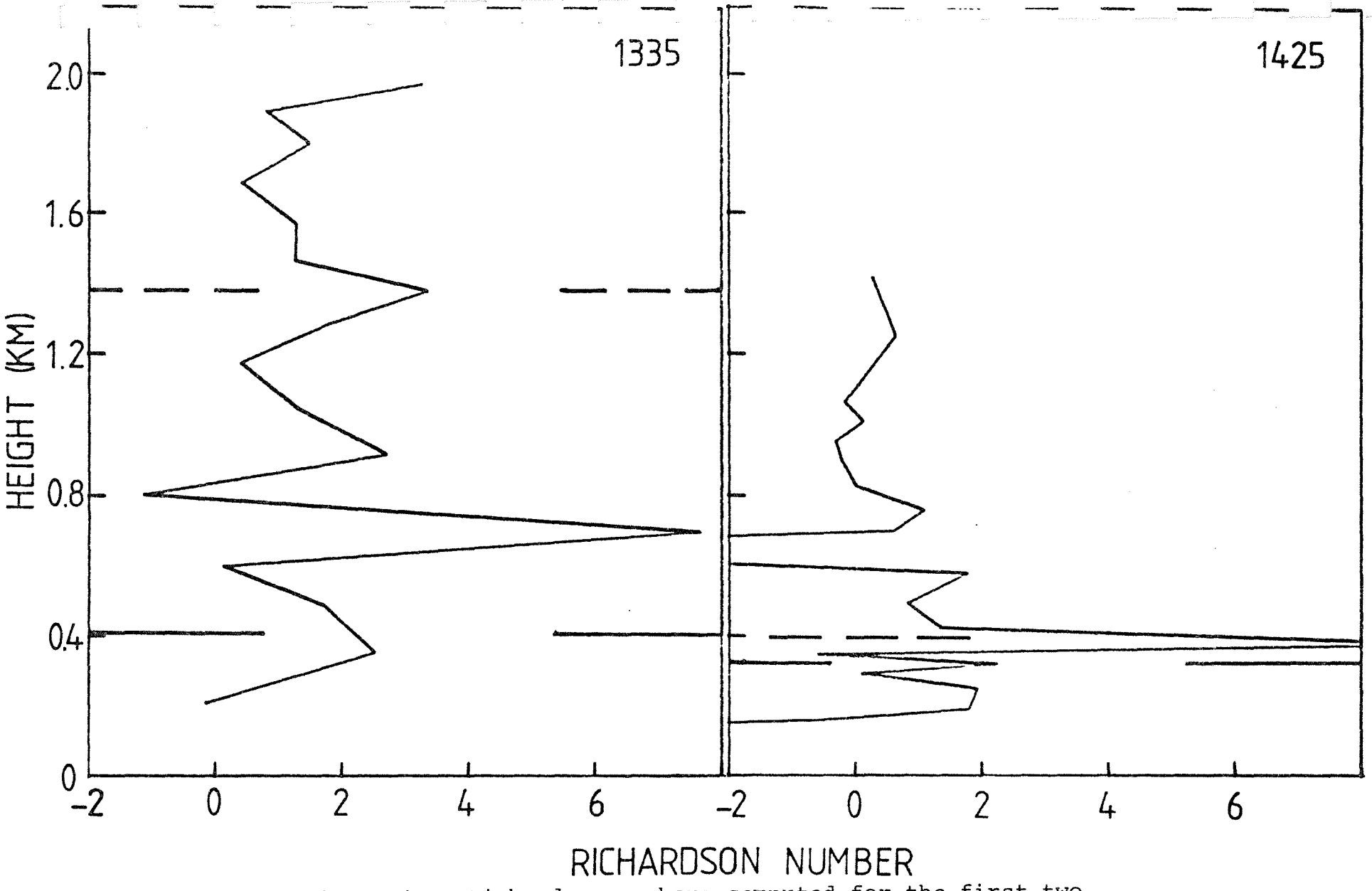

Figure 4: Richardson numbers computed for the first two temperature records provided by the 31st January Kwinana sonde releases. The upper limit for development of spontaneous instability is 0.2,well below the range detected. The broken lines show mixing depths computed using an adiabatic model of plume ascent, while the continuous horizontal lines show the results of use of an entrainment model (see text)

MIXING DEPTHS AT KWINANA, 31ST JANUARY 1980

2. Mixing Depth Models

P.J. Rye

INTRODUCTION

The growth of mixing depth for onshore airflows has often been related directly to the effects of surface temperature inland, producing either empirical or theoretical models (e.g. Fritz, et al, 1980). To evaluate the possibility of using such techniques at Kwinana, for application in pollutant dispersal modelling, a theoretical model has been developed.

The output of the model is compared to mixing depths computed by a numerical seabreeze model (Rye, 1980), which uses a totally different approach, to measurements at the Alcoa Mudlake and Hope Valley Base Station sites on 31st January 1980, and to measurements at the former site on 2nd March 1978.

OUTLINE OF MODEL

When the sea breeze arrives at the coastline it is generally stable, but with no sudden rise of temperature with height. The "sea breeze inversion" is subsequently produced as mechanically and thermally induced turbulence mixes the lower levels to give a uniform potential temperature.

The assumption of uniformity of potential temperature within the mixed layer, together with models for the surface heat flux and flux of heat entrained out of the layers above the mixed layer, allowed computation of its growth.

By assuming the onshore flow to have a horizontally and vertically uniform velocity, it was possible to convert the resulting time evolution of the mixed layer to a change with distance downwind from the coast. The appendix gives the method used for the calculation of time evolution, and measured winds were used to derive the mixing depth/distance inland connection.

The parameters of the model were wind speed, surface flux, date and time of day inflow stability and ratio of entrained to surface flux (B/(1-B) in the appendix). Surface fluxes were assumed to vary sinusoidally between sunrise and sunset with a noon peak varying from 300 Wm^{-2} in winter to 600 Wm^{-2} in summer. Time of day was specified on the "Roman clock" with 12 hours from sunrise to sunset. The value of B was derived from the results of Deardorff (1980), whose estimate fell in the mid-range of other measurements. Inflow stability in the absence of other data, was obtained directly from the output of a seabreeze model (Rye, 1980).

RESULTS AND DISCUSSION

The results of modelling the mixed layer on 31st January 1980 are shown in figure 1. A surface flux of 493 Wm^{-2} was used, with the lapse rate and wind speed shown.

Also shown, by crosses, are the mixing depth computed by the sea breeze model at 2.5 km and 7.5 km inland - that is, 5 and 15 km downwind on the 210° wind direction. Agreement is excellent - in fact, surprisingly good considering the 5 kilometre horizontal resolution of the model. A careful study of the temperature profiles at 2.5 and 7.5 km inland, produced by the sea breeze model (figure 2), has shown that the 2.5 km value is likely to be an underestimate, due to the strong effects of cool air advection on modelled plume temperature. However, the 7.5 km value of about 420 m is in good agreement with the mixed-layer model.

For wind directions between 210° and 230° the Alcoa Mudlake site is about 15 km downwind from a landfall on Warnbro Sound. The Hope Valley base station is similarly about 13 km 'inland'. This explains why, despite being less than half as far from the coastline, the acoustic sounder at Hope Valley recorded similar mixing depths to those measured at the Mudlake. In both cases, the measured values of 400-450 m were in good agreement with the theoretical calculations, both of 420 m.

A comparison was also carried out between the model calculations and the sea breeze data of 2nd March, 1978. These showed a mixing depth over the radiosonde site of 550 metres for a wind speed of 5.8 ms^{-1} and stability of 0.009° Cm^{-1}), again very close to the radiosonde measurement of 500-550 m.

Two questions arise from this analysis. Firstly, the 320 metre value measured by the third radiosonde release is not consistent with model results - the probable answer to this problem lies in the requirement of vertically and horizontally uniform winds. At about 1430, the sea breeze was still returning to its 'undisturbed' mode after the disruption at about 1335 (see p.35). It is likely that subsidence or warm air advection could have modified the stability of the inflow air.

Secondly, the easy reproduction of mixing depths seems to suggest an overall constancy of inflow stability in the sea breeze. Whether this is a fully general rule is dubious, but qualitative considerations can be used to suggest some "negative feedback" controls on the variability of this parameter.

CONCLUSIONS

The sea breeze model and mixed-layer models discussed have both shown considerable skill in modelling mixing depths over Kwinana. While some secondary questions remain, it appears likely that both will be useful in analysing pollutant dispersal in the Kwinana area.

REFERENCES

Deardorff, J.W. 1980 "Laboratory Study of the Entrainment Rate in a Convectively Mixed Layer", Third Conference on Ocean-Atmosphere Interaction, January 30 - February 1, Los Angeles, Calif. (Abstracted in Bull. Am. Met. Soc. 60, p. 1251).

Fritto, T.W., F.J. Starheim and B.J. Diehl 1980 "A Formulation for Defining the Development of the Thermal Internal Boundary Layer (TIBL) in Sea Breeze Flows", second Conference on Coastal Meteorology, January 30 - February 1, Los Angeles, Calif.

Rye, P.J. 1980 "A Model for Pollutant Transport by the Sea Breeze. 1 Structure and Validation of Sea Breeze Model". Manuscript available from author.

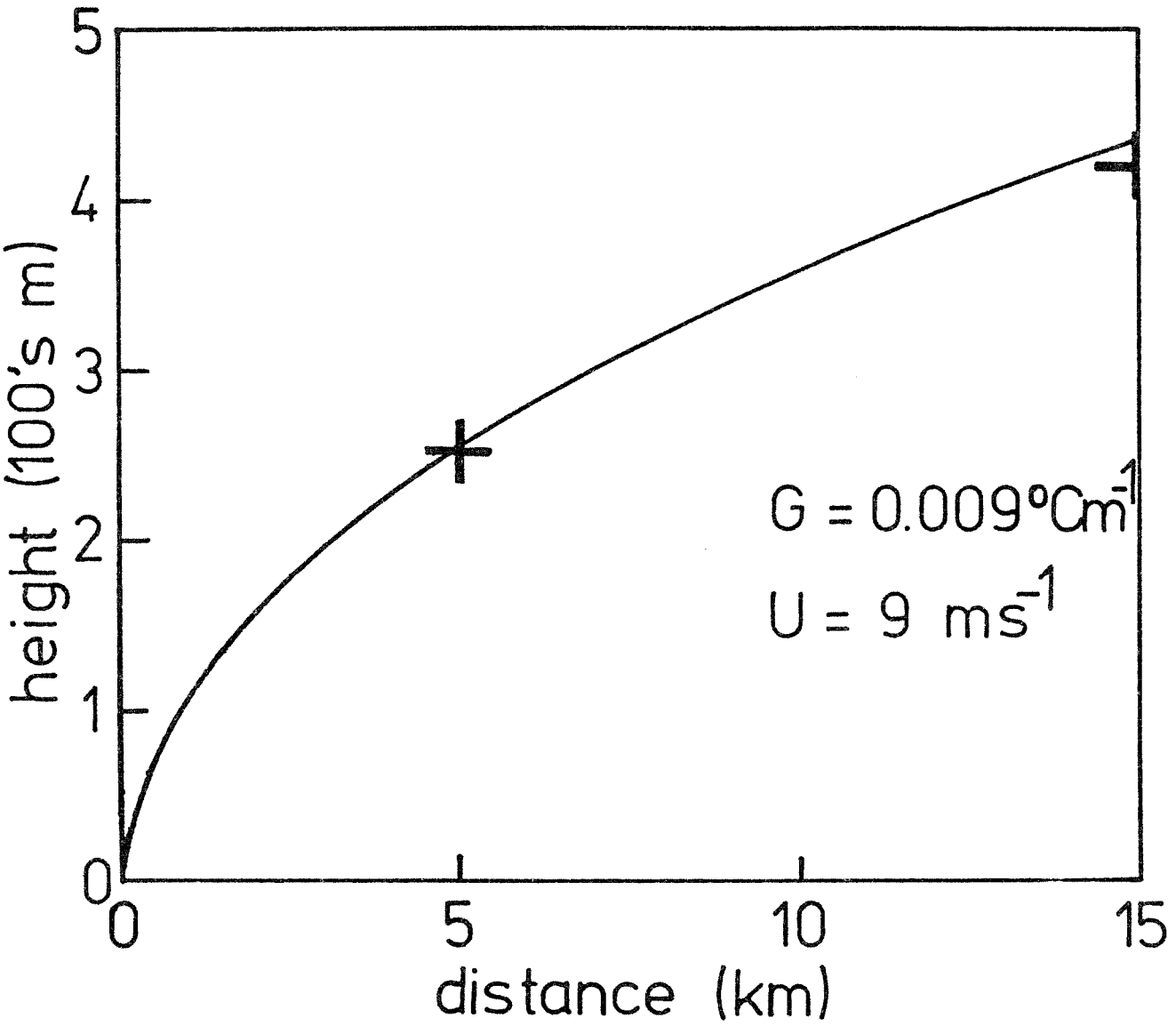

Figure 1: Mixing depth computed as a function of distance inland, for conditions representative of the 31st January, 1980, sea breeze. The crosses are the values computed by a sea breeze model (see text).

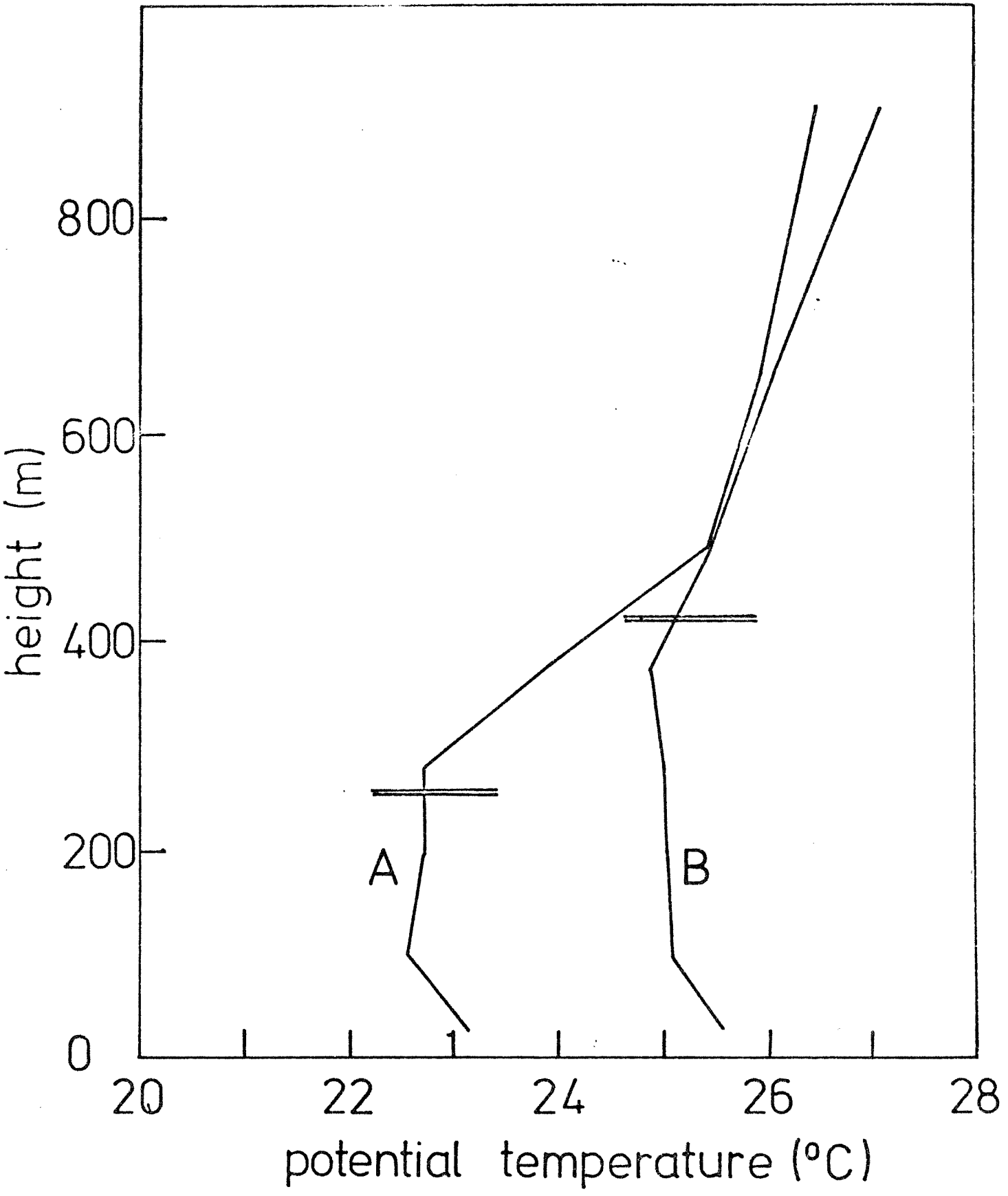

Figure 2: Temperature profiles computed by a numerical sea breeze model, at 1430 W.S.T. on 31st January 1980. Distances inland are 2.5 km (A) and 7.5 km (B). Mixing depth estimates are shown by double horizontal lines.

APPENDIX

BOUNDARY LAYER EVOLUTION

The aim of the model described below is to compute how mixing depth increases with time, from a defined initial state. The externally specified parameters are:

Q_t	surface temperature flux, in $^oC\ ms^{-1}$
G	potential temperature gradient, $^oC\ m^{-1}$
B	turbulent entrainment parameter, equal to the ratio of turbulent flux to surface flux.
B'	B/(1+B)
H_o	mixing depth when computation starts
Θ_o	boundary layer potential temperature when computation starts

Model variables are:

H	mixing depth
Θ	boundary layer potential temperature
$d\Theta_i$	potential temperature rise at the inversion

We assume that at the start of computation, inversion strength is zero ($d\Theta_i = 0$). Thus, the potential temperature profile evolves as shown in figure 1, which shows profiles at time 0 (start), t, and t + dt.

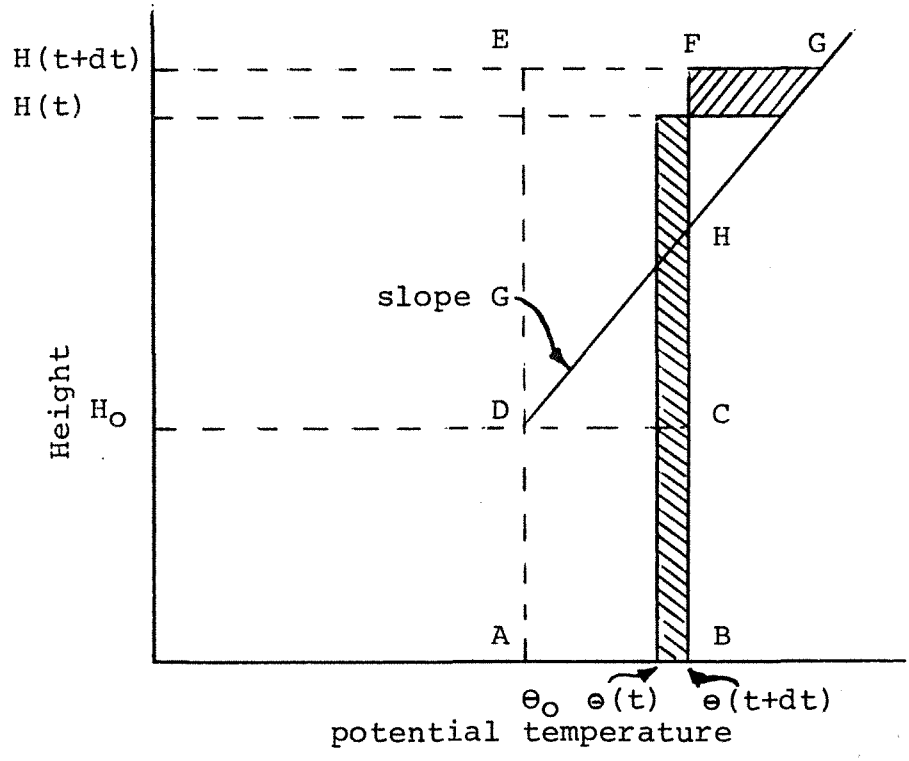

Figure 1. Schematic of boundary layer model construction

The fundamental heat balance is therefore given by the opposing contributions of the hatched areas of figure 1, so that

$$H\, d\theta/dt - d\theta_i\, dH/dt = Q_t \qquad (1)$$

The value of $d\theta_i$ may be related to other variables, through

$$d\theta_i = G(H - H_o) - (\theta - \theta_o) \qquad (2)$$

and simple geometry shows that the total heat,

$$Q = \int Q_t\, dt$$

is given by

$$Q = \text{area ABCD} + \text{area DCH} - \text{area FGH}$$

while

$$H\,(\theta - \theta_o) = \text{area ABCD} + \text{area DCH} + \text{area DHFE}$$

so

$$H\,(\theta - \theta_o) - Q = \text{area DHFE} + \text{area FGH}$$

$$= \tfrac{1}{2}G(H - H_o)^2 \qquad (3)$$

Differentiating,

$$H\, d\theta/dt + (\theta - \theta_o)\, dH/dt = Q_t + G(H - H_o)\, dH/dt \qquad (4)$$

From the closure hypothesis,

$$(d\theta_i\, dH/dt)/(H\, d\theta/dt) = B^1 = \text{constant} \qquad (5)$$

so that, from (1),

$$H\, d\theta/dt - B^1 H\, d\theta/dt = Q_t$$

and thus

$$H\, d\theta/dt = Q_t/(1 - B^1) \qquad (6)$$

Together, (6) and (4) give

$$Q_t/(1 - B) + (\theta - \theta_o)\, dH/dt = Q_t + G(H - H_o)\, dH/dt \qquad (7)$$

so $$\left[G(H - H_o) - \frac{Q_t + \tfrac{1}{2}G(H - H_o)^2}{H} \right] dH/dt = Q_t\, B^1/(1 - B^1)$$

from (3)

Therefore, $B\ Q_t = \frac{1}{H}\frac{dH}{dt}\left(GH(H - H_o) - Q - \tfrac{1}{2}G(H - H_o)^2\right)$

$$= \frac{1}{H}\frac{dH}{dt}\left(G(H - H_o)\ (H - \tfrac{1}{2}H + \tfrac{1}{2}H_o) - Q\right)$$

$$= \frac{1}{H}\frac{dH}{dt}\left(\tfrac{1}{2}GH^2 - \tfrac{1}{2}GH_o^2 - Q\right)$$

$$= \frac{G}{2H}\frac{dH}{dt}\left(H^2 - (H_o^2 + 2Q/G)\right) \qquad (8)$$

In the case of a uniform sea breeze flow, $H_o = 0$ and $Q = t\ Q_t$. Thus

$$H\frac{dH}{dt} - \frac{2 + Q_t}{G}t\ \frac{1}{H}\frac{dH}{dt} = \frac{2BQ_t}{G}t \qquad (9)$$

which is solved by the expression

$$H^2 = 2\ t\ (1 + B)\ \frac{Q}{G}t$$

$$= 2\ (1 + B)\ \frac{Q_t}{G}\frac{x}{U} \qquad (10)$$

where x is inland distance and U wind speed.

EVALUATION OF A GRID DISPERSION MODEL USING THE 31ST JANUARY TRACER RELEASE

P.J. Rye

1. INTRODUCTION

A dispersion model using a three-dimensional rectilinear grid has been created to evaluate the mesoscale effects on pollutant dispersal of the passage inland of the sea breeze. The version described in this paper is designed to use as input data, the wind and stability parameters generated by a numerical sea breeze model (Rye, 1980).

Although it was created to represent phenomena at larger ranges and of broader scales than the plume detected during the tracer release conducted on the 31st January, 1980, the data obtained in this study represented a stringent test of the ultimate capabilities of the model. It allowed the detection of small inconsistencies, pointing to inadequacies in the modelling techniques used, and in return the model showed the importance of the coastal fumigation process in producing large groundlevel concentrations several kilometres away from the source.

2. STRUCTURE OF MODEL

The basis of the pollutant dispersal model is a three-dimensional grid, of size 15 x 15 points horizontally, and of four layers vertically. Processes represented are advection (horizontal and vertical) and lateral and vertical dispersion. Emissions from sources in the area covered by the model are included by their insertion at a level corresponding to the ultimate rise of their plumes.

a) Advection

Horizontal and vertical transport of pollutants are represented using the approach based on the split explicit scheme described by Gadd (1978,1980). For simplicity, advection in each of the x- and y- directions, parallelling the grid axes, is computed separately, giving a fully-split algorithm. This is necessary to allow for the effects of spatially-varying wind velocities, which were not included in Gadd's description, and to improve the speed of execution of the program.

Winds are interpolated from the data fields at the boundaries of each cell of the dispersal model, giving values with half-integer subscripts (See Fig. 1). The sea breeze is assumed uniform in a north-south direction, so that velocities only vary in the x- direction and the calculation of advection in the y- direction is somewhat simplified.

Thus, the concentration Q at time $(n+1)Dt$ is derived from the values at time nDt and the horizontal velocity (u, v), where Dt is the time step, using the following formula:

$$
\begin{aligned}
Q_j^{n+1} &= Q_{J-2}^{n} \left[-M_j \; 1/6 \; (1 + M_{j-3/2})\right] \\
&+ Q_{J-1}^{n} \; M_j/2 \left[1 + 2a/3 + M_{j-1/2}(1 + a) + M_{j-3/2}\, a/3\right] \\
&+ Q_j^{n} \left[1 - M_j^2 (1 + a)\right] \\
&+ Q_{J-1}^{n} \; M_j/2 \left[-1 - 2a/3 + M_{j+1/2}(1 + a) + M_{j+3/2}\, a/3\right] \\
&+ Q_{J+2}^{n} \left[M_j \; a/6 \; (1 - M_{j+3/2})\right] \qquad (1)
\end{aligned}
$$

Where $M_{j+1/2} = u_{j+1/2}\, Dt/Dx$ or $v_{j+1/2}\, Dt/Dy$, Dx and Dy being the x- and y- grid intervals, $M_j = (M_{j-1/2} + M_{j+1/2})/2$ for integer j, and $a = 3/4\,(1 - M_j^2)$.

In use, the above formula is firstly applied to rows in the x- direction, and subsequently to rows in the y- direction. A test of this simplified approach, in situations typical of wind fields at Kwinana, showed it to possess relatively high accuracy up to M values of 0.8 and a considerable advantage in execution time over Gadd's full two-dimensional scheme.

Vertical advection is included in a much simpler form, since its effects are expected to be always secondary to turbulent diffusion. Intervals in the x- direction are selected for consistency with sea breeze model height intervals, so that any vertical velocity $w_{i,k}$ is to good approximation, applicable to the top of layer k of the dispersion model. Thus, vertical advection could be adequately represented by

$$
\begin{aligned}
Q_{i,k}^{n+1} &= Q_{i,k}^{',n} + (w_{i,k}\,(Q_{i,k+1}^{',n} - Q_{i,k}^{',n}) + w_{i,k-1}\,(Q_{i,k-1}^{',n} \\
&- Q_{i,k}^{',n}))/Dz_k \qquad (2)
\end{aligned}
$$

where Q' is the value prior to the inclusion of vertical advection, and Dz_k is the thickness of layer k.

b) Lateral Dispersion

The physical processes of lateral dispersion are, in general, of much smaller magnitude than numerical diffusion introduced by the finite difference algorithm used. The approach below is therefore applied only in restricted circumstances, as subsequently explained (see Section 3).

Finite-difference grid models m ust represent the dispersion of plumes using some form of eddy diffusivity - even high-order closure models (e.g. Donalson 1973). The first-order closure used here has, as input parameters, mixing depth (h), Monin-Cbukhov length (L) and friction velocity (U_*). To derive the required lateral diffusivity, it was first noted that velocity perturbations in an unstable boundary layer were characterised by a standard deviation (Panofsky et al, 1977).

$$\sigma_v = U_* \, (12 - 0.5 \, h/L)^{1/3} \qquad (3)$$

for z less than h. These pertubations vary on a time scale related to the Lagrangian time scale of the flow (e.g. Sawford, 1979).

Such a set of random perturbations can be modelled by a set of random velocities constant over a fixed time, proportional to the Lagrangian time scale. The change in concentration at a grid area i ("i" representing either an x- or y- position) due to motion of pollutants from area i-1 is related to the probability that, due to such a random velocity to the area i. That is, the diffusion contribution to the change in C_i will be

$$dQ_i = \int_0^{Dx} Q(s) \; P \; (v_{turb} \, Dt > s \text{ and } v_{turb} \, Dt < s + Dx) \; ds \qquad (4)$$

We can assume that the value of Q within $0 < s < Dx$ is uniform, since the finite difference grid contains no other information. The turbulent velocity v_{turb} is taken to have a Gaussian distribution, with standard deviation given by equation (3), so that

$$P(v_{turb} \, Dt > s) = \frac{1}{(2\pi)^{1/2}} \int_{s/Dt}^{\infty} \exp(-r^2/2\alpha_v^2) \, dr$$

$$= \Phi \, (s/Dt) \qquad (5) \qquad (5)$$

Thus, noting that we can rephrase equation (4) by

$$dQ_i = \int_Q^{Dx} Q(s)\ P\ (v_{turb} Dt > s)\ ds - \int_O^{Dx} Q(s)\ P(v_{turb} Dt > s + Dx)\ ds$$

$$= Q_{i-1} \left(\int_O^{Dx} \Phi\ (s/(\sigma_v Dt))\ ds - \int_O^{Dx} \Phi\ ((S + Dx)/(\sigma_v Dt))\ ds\right.$$

$$= Q_{i-1} \left(\int_O^{Dx/(\sigma_v Dt)} \Phi\ (r)\ dr - \int_{Dx/(\sigma_v Dt)}^{2Dx/(\sigma_v Dt)} \Phi\ (r)\ dr\right)\ \sigma_v\ Dt/Dx \qquad (6)$$

Equation (6), involving integrals of a function for which no closed expression exists, is not amenable to exact solution. However, noting that in normal circumstances σ_v is about $(u^2 + v^2)^{1/2}/4$ and that for computational economy the maximum of uDt/Dx and vDt/Dy is maintained at about 0.8, we see that :

$$(Dx \text{ or } Dvl/(\sigma_v Dt) = 4\ (Dx \text{ or } Dy)/([u \text{ or } v] Dt) \qquad (7)$$

$$> 5.6$$

Therefore, the second term in the right hand side of equation (6) is negligible, and that the first term is, in normal circumstances, nearly a constant, giving

$$Q_i = Q_{i-1}\ \sigma_v\ Dt/Dx \int_O^{infinity} \Phi\ (r)\ dr$$

$$= \frac{1}{(2\pi)^{1/2}}\ \sigma_v\ Dt/Dx \qquad (8)$$

The above model therefore gives, for integrations over a time step governed by the Lagrangian time scale, an effective lateral diffusivity

$$K = \sigma_v\ Dx/(2\pi)^{1/2} \qquad (9)$$

c) Vertical Dispersion

Vertical transport is estimated using a first-order eddy diffusivity model, extrapolated from surface layer expressions and compatible with the expressions used by Rye (1981). Vertical dispersion is related to the transfer coefficient for heat, K_H,

$$K_H = U_* \, l/\phi_H \tag{10}$$

where K_H is the eddy diffusivity, the dimension less profile function. The mixing length, l, is expressed in the form

$$l = \begin{cases} kz\,(1 - z/H)^{3/2} & z < H \\ 0 & z > H \end{cases} \tag{11}$$

where H is the creater of the mixing depth and L, and the exponent 3/2 was chosen to give acceptable agreement with measurements (e.g. Hanna 1978). The form of ϕ is chosen to be consistent with surface values at low level, and with convection in unstable conditions at heights larger than -L. The form chosen is therefore

$$\phi_H = (1 - 24\, z/L)^{-1/3} \tag{12}$$

In stable conditions, the form chosen is

$$\phi_H = (1 + 5.7\, z/L)/(1 + z/L) \tag{13}$$

d) Emissions Inventory

In normal operation, all 43 sources in the full Kwinana emissions inventory are used. During this mode, and in the experiment described subsequently, plume rise is calculated in accord with the neutral-conditions formula of Briggs (1969), namely

$$Z = 1.6\,(F\, x_p^2)^{1/3} / (u^2 + v^2)^{1/2} \tag{14}$$

where the stack flux term, F, is given by

$$F = gq/(\pi \rho_a C_p T_p) \tag{15}$$

and x_p is the distance at which plume rise stops (10 times stack height), q is the heat emission rate, ρa is the plume density, C_p the specific heat and T_p the temperature of the plume.

During the sea breeze periods, the onshore flow is normally stable. However, for typical stabilities of about 1 degree Celsius per 100 metres and inflow speeds of 6 to 10 m s^{-1}, the ultimate plume rise derived from Briggs' stable-conditions formula was greater than that given for neutral conditions. It was therefore concluded that inflow layer stability was of little relevance in plume dynamics, and the stable conditions formula always used.

In use, the above plume rise is added to the stack height to derive an emission level for the source. The emission from each stack is then added to the layer of the model, in which its emission level is located. This approximation is considered satisfactory, since the model was developed to study phenomena occurring at a large distance from the sources.

3. INITIALISATION

In normal use, grid-type models possess an inherent error, due to spurious diffusivity resulting from the limited resolution of space and time scales. However, the advection scheme used possessed the feature that, when pollutants were transported through one gridlength in one time step, this error was reduced to zero.

Thus, the model was initialised using x- and y- increments of 450 and 800 metres, and a time step of 100 seconds. With x- and y- wind components of 4.5 and 8 ms^{-1} respectively, exact advection was produced.

The dispersion parameters used were derived from both sea breeze-model output and from base station data. The 12-level sea breeze model showed a mixing depth of 260 metres at 2.5 km inland, and 420 metres at 7.5 km inland (the latter in excellent agreement with measurements at Alcoa Mudlake F by radiosonde for most of the afternoon - see pp. 34 - 36 - and the former agreeing well with theory). An "$x^{\frac{1}{2}}$" law gave values at the required intervals inland. Both the estimates of surface roughness in the sea breeze model, and the measurements made using the 27-metre tower at Hope Valley (Fig. 2) implied drag coefficients of just over 0.01, and hence a friction velocity of 1 ms^{-1} was used. Measurements of the Monin-Obukhov length taken from the data obtained at the same tower centred around -130 metres at the time of the release, in fair agreement with expected values of about -150 metres. (Fig. 3). Thus, the dispersion parameters could be summarised as:

$$u = 4.5 \text{ ms}^{-1}$$

$$v = 8.0 \text{ ms}^{-1}$$

$$w = 0.0$$

$$U_* = 1.0 \text{ ms}^{-1}$$

$$L = -150.0 \text{ m}$$

$$h = (23.52m.x)^{\frac{1}{2}}$$

The variations of wind in the vertical, and of wind, L and U_* horizontally, were not considered. In view of the insensitivity of dispersion on L (plume width depending on only the one sixth power of -L), of the unknown variation of roughness on distance inland, and of the approximate uniformity of wind in the inflow layer, this approximation was considered adequate.

The data used for validation of the dispersion calculation were the measured emission rate of Freon-11 from the 140 metre S.E.C. stack (0.0851 kg s^{-1}) and the maximum ground-level concentrations detected at each monitoring site. As discussed below, the latter data were contoured independently of Dr. Bruce Hamilton's analysis, to ensure mass-flux consistency.

4. RESULTS AND DISCUSSION

Figure 4 shows the computed ground-level concentrations, which may be compared to the measurements presented in Figure 5. The overall agreement is encouraging, but some comments on discrepancies are appropriate.

The peak concentration computed, of 20 μg m^{-3}, is somewhat below the measured peak of about 30. This may be partly due to the inability of the model to resolve features of size less than the gridlength, but is no doubt augmented by the necessity to limit the value of K Dt/Dz^2 used in vertical dispersion. Were this allowed to exceed one half, numerical instability would result in the present model, and its value is therefore arbitrarily restricted to a maximum of a half. With these restrictions in mind, the agreement at short range is felt to be excellent - particularly as the model predicts the location of the maximum with good accuracy.

At larger distances inland, the agreement initially improves but the broadening of the 10 μg m^{-3} contour results in measureable errors at the edge of each plot. It is readily shown, however, that errors in the data reduce its value here.

If we take values across the outermost rank of data points, and fit a Gaussian curve through the data, it is possible to estimate a centreline value of 15 to 22 μg m^{-3}, and a plume standard deviation of about 1000 metres. Thus, from the requirements of mass continuity in a well-mixed boundary layer, the mixing depth is related to this value (q_0), the standard deviation (σ), the pollutant flux (f) and wind speed (U) by

$$h = \frac{f}{q_0 U (2\pi)^{\frac{1}{2}} \sigma}$$

$$= \frac{0.0851}{(15 \times 10^{-9})\ (9)\ (2.5066)\ (1000)}$$

$$= 251 \text{ metres}$$

It should be noted that this is the maximum that can be derived, 15 $\mu g\ m^{-3}$ being the lowest estimate of q_0, and all contours indicating lower values than, for example, those of Dr. Bruce Hamilton. Thus, either σ is too large (an unlikely error, since the required 600 metres is clearly too small), or q_0 should be about 10 $\mu g\ m^{-3}$.

It is suggested that the 9.79 $\mu g\ m^{-3}$ value is inaccurate, and also that the proposed 320 metre mixing depth is more correct than the 400 metre value used in the model. A possible combination in reasonable consistency with the data is then an "h" of 320 metres, a "σ" of 900 metres and a "q_0" of 13 $\mu g\ m^{-3}$.

A mixing depth of 420 metres could be fitted with a q_0 of 12 $\mu g\ m^{-3}$ and a σ of 750 metres. However, this would require the 7 $\mu g\ m^{-3}$ contours to be only 3 cm apart on figure 3, at the line of the outermost data points - an unlikely possibility.

Figure 6 shows the variation of Freon concentration along vertical and horizontal axes. The fumigation of the area below where the plume axis intersects the top of the mixed layer is shown clearly, as is the progressive dispersion of Freon to greater depths as the plume moves inland. The rapid development of uniform vertical mixing of the plume is also noticeable.

5. FUTURE IMPROVEMENTS

The analysis discussed above has shown the model to possess significant strengths in representing the dispersal of pollutants at Kwinana, but further refinements have been considered.

Panofsky (private communication) has suggested that the similarity of the topography at Kwinana to one of the sites where his own dispersion measurements were made might mean that an increase in the value of horizontal dispersion coefficient will be necessary. In particular, the coefficient 12 in equation (3) may need to be increased to as much as 25. The present validation data are inadequate to resolve the resultant effects on concentrations, but the change seems logical on his evidence.

A suggestion arising from the 16th May seminar was also considered. Dr. Tom Lyons drew attention to the possibility of using a linear gradient, rather than a discontinuous step, to estimate the motion of pollutants between grid squares. A repeat of the analysis described in section 2(c), using this alternative, showed that the resulting model for K was

$$K = \sigma_v\ DX/2$$

This alternative would not greatly affect plume widths, but in principle would improve the accuracy of representation of dispersion on uniform gradients and worsen it at the locations of concentration peaks.

As may be seen in Figure 4, the model allows the dispersion of pollutants into the entire depth of any layer into which the top of the mixed layer penetrates even slightly. This results in significant errors at the coarse vertical resolution used. A proposed modification would increase the concentration estimate used in the vertical dispersion calculation (only) by the ratio of layer depth to the height of the mixed layer top above the layer's lower edge. This would remove the error.

6. CONCLUSIONS

The model described above has shown the intended accuracy at large ranges from the source, giving computed centreline concentrations and plume widths within the range of uncertainty of validation data. As a bonus, at short ranges it demonstrates clearly the effects of fumigation by the plume as the mixing depth increases inland. The accuracy with which it represents this process is better than that of conventional Gaussian dispersion models.

7. REFERENCES

Briggs, . 1969. "Mathematical Analysis of Chimney Plume Rise and Dispersion". Phil. Trans. Roy. Soc. Lond. A265, pp. 197-203.

Donaldson, C. dup. 1973. "Construction of a Dynamic Model of the Production of Atmospheric Turbulence and Dispersal of Atmospheric Pollutants", Workshop on Micrometeorology, A.M.S. Boston.

Gadd, A.J. 1978. "A Split Explicit Integration Scheme for Numerical Weather Prediction:, Quart. J.R. Met. Soc. 104, pp. 569-582.

Gadd, A.J. 1980. "Two Refinements of the Split Explicit Integration Scheme", Quart. J.R. Met. Soc. 106, pp. 215-220.

Hanna, S.R. 1978. "A Review of the Influence of New Boundary Layer Results on Diffusion Prediction Techniques", W.M.C. Symposium on Turbulence and Diffusion, Norrkoping, pp. 119-126.

Ranofsku, H.A. C.A. Eqolf and R. Lipschutz. 1978. "On the Characteristics of Wind Direction Fluctuations in the Surface Layer", Bound. Layer Met. 15. pp. 439-446.

Rye, P.J. 1981. "A Model for Pollutant Transport by the Sea Breeze. 1. Structure and Validation of Sea Breeze Mode." Manuscripts available from author.

Sawford, B.L. 1979. "Wind Direction Statistics and Lateral Dispersion". Quart. J.R. Met. Soc. 105, pp. 841-848.

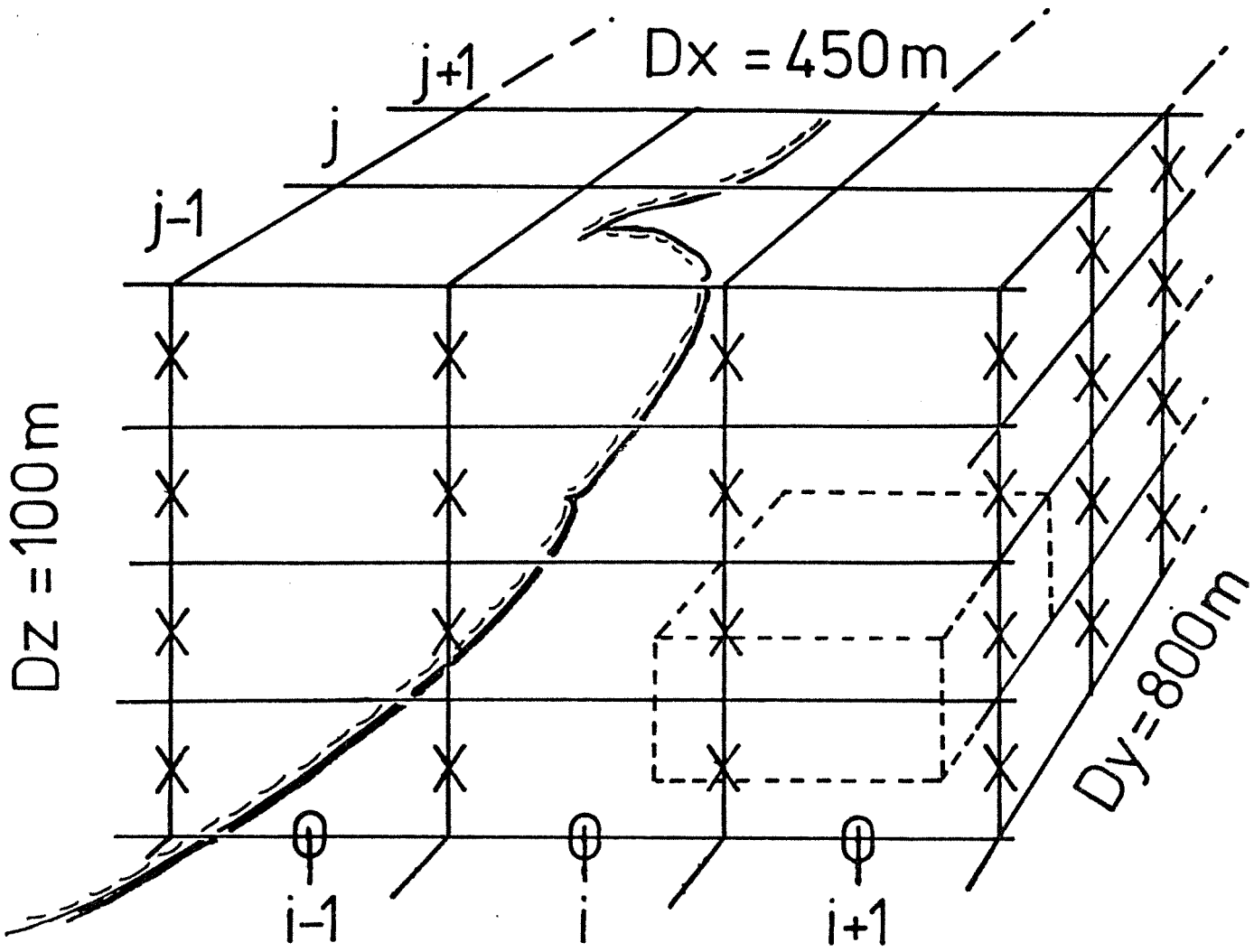

Figure 1: Schematic of grid and data structure of model. The points X are those at which wind field values are interpreted, while the points O are those at which U_*, h and L are retained. The computed value of concentration Q would thus be the average within the box showing $Q_{i+1,j^{-2},2,\ j-1,2}$, by the broken line.

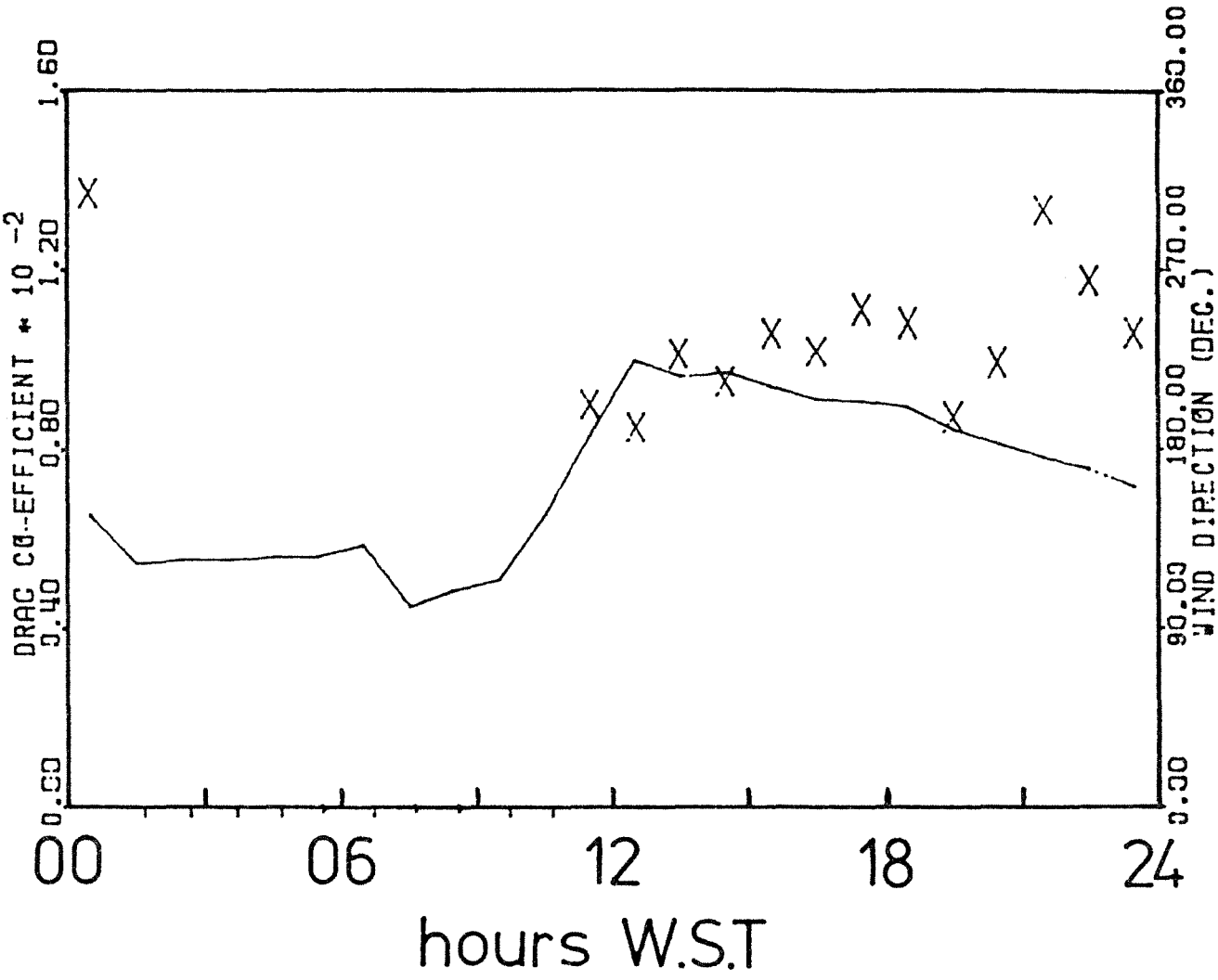

Figure 2: Drag coefficient (marked X) as a function of time on 31st January, with wind direction (continuous line) shown to allow relation of data to the sea breeze. Both variables are averaged over one hour periods, and the 27 metre data logger was inoperative prior to mid-day.

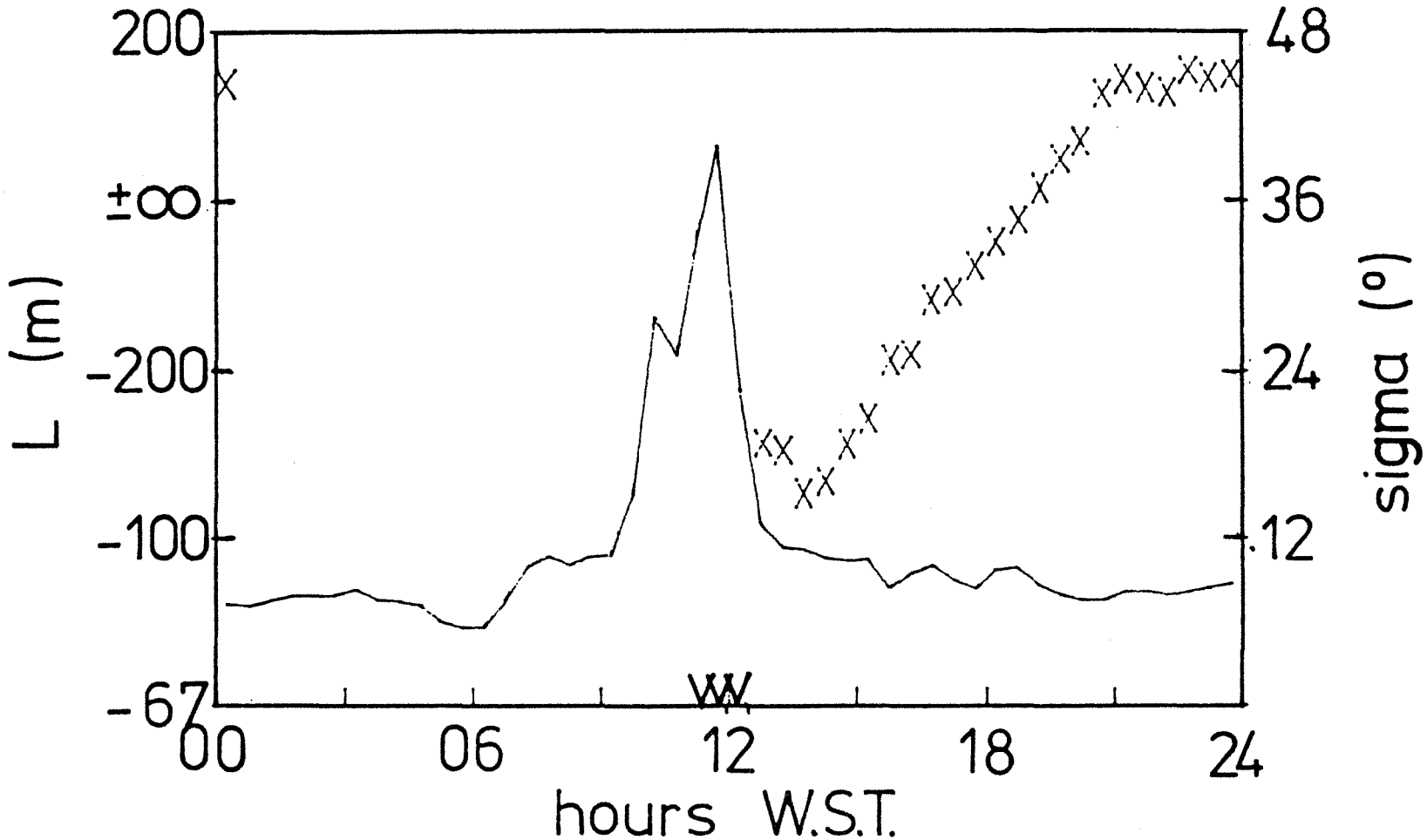

Figure 3: Monin-Ohukhov length Lasa function of time on 31st January, with wind direction standard deviation (continuous line) shown to illustrate its connection with L. Both variables are averaged over half-hour periods, the former shown by crosses and the latter by a continuous line. Note that the left hand scale is hyperbolic.

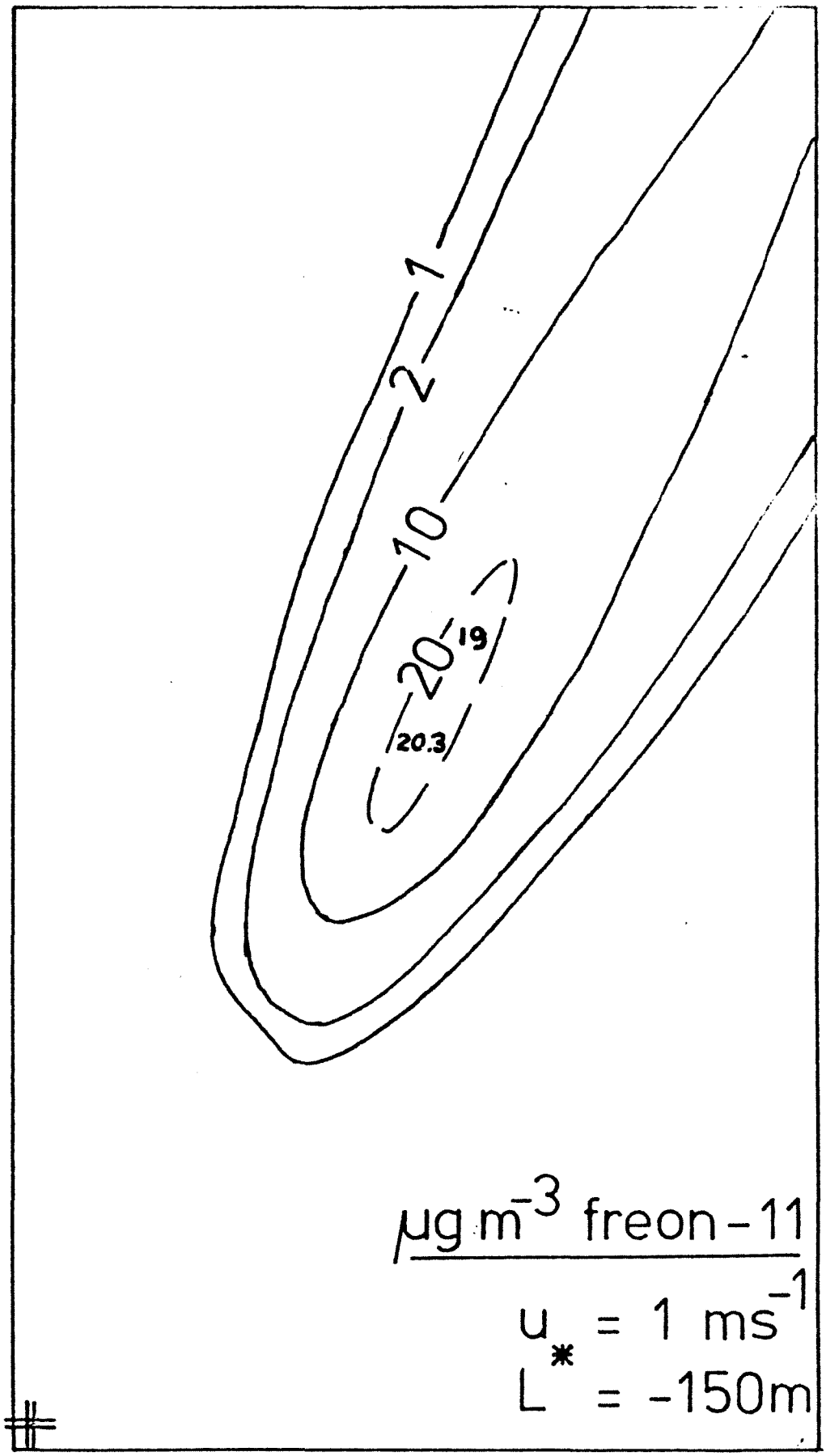

Figure 4: Computed ground level concentrations of freon-11. The "19" and "20.3" represent grid-square means on the plume axis, boty implying peaks within their squares in excess of 20 μg m^{-3}. Map scale 1:50,000.

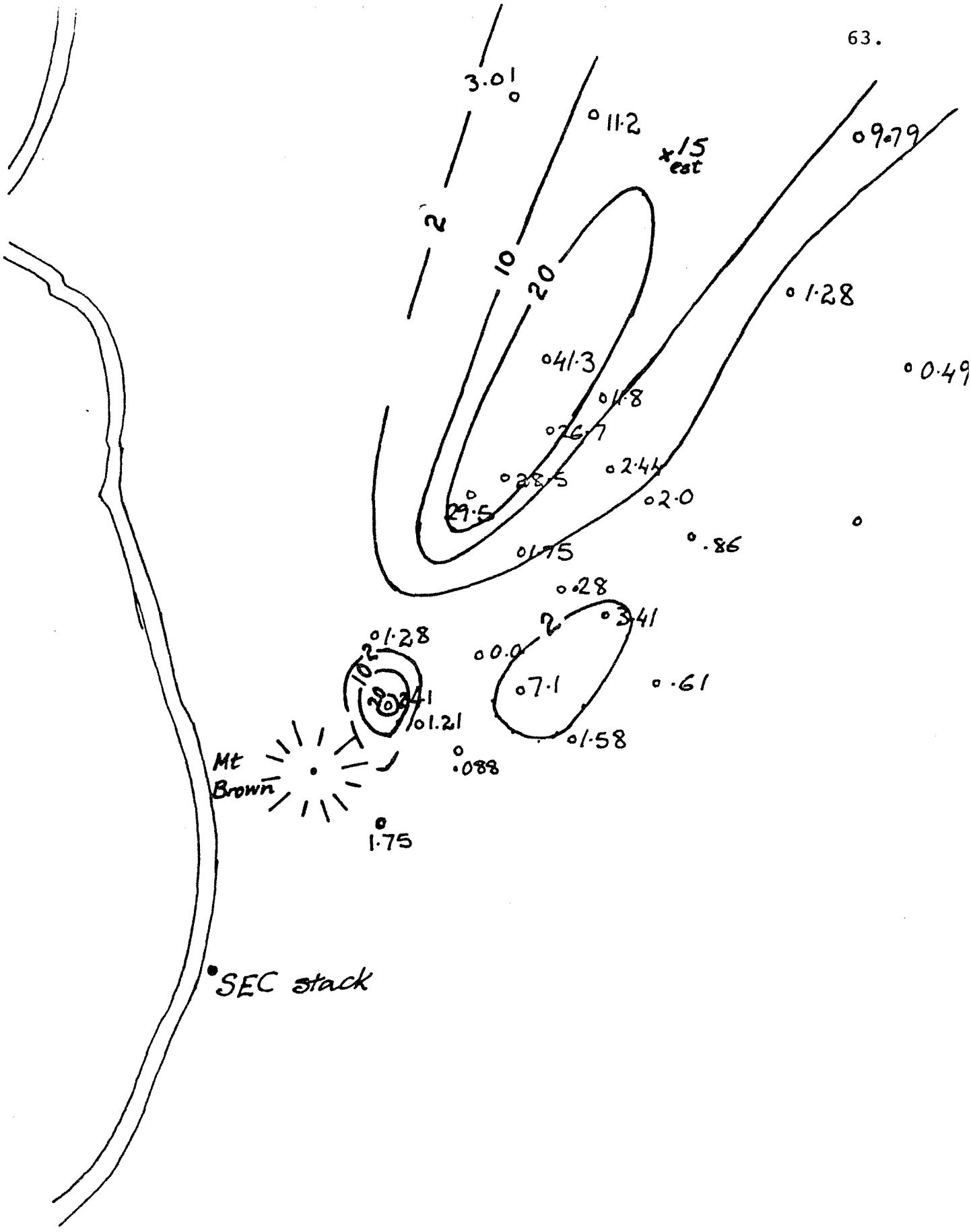

Figure 5: Measured maximum froen-11 concentration (μg m^{-3}) at sites shown, on same scale as figure 4. The 15 est. value on the plume axis was derived from nearby values (see text for explanation).

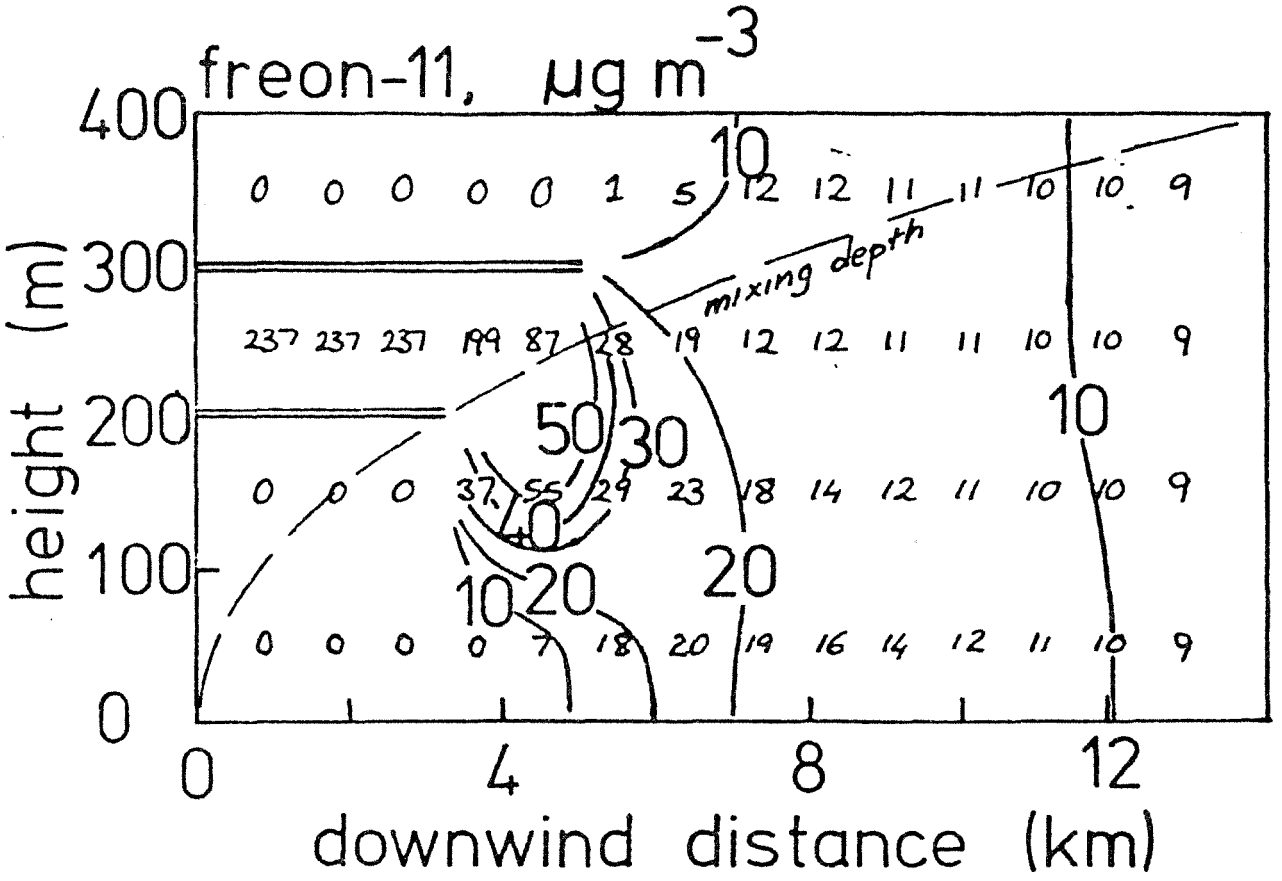

Figure 6: Cross-section showing grid-square mean concentrations computed along the plume axis. The mixing depth used is shown as a broken line.